Author Manuscript
Author Manuscript
Author Manuscript
Author Manuscript

HHS Public Access
Author manuscript
Front Trop Dis. Author manuscript; available in PMC 2023 February 17.

Published in final edited form as:
Front Trop Dis. 2023 ; 3: . doi:10.3389/fitd.2022.1011124.

Discovery of pyrazolopyrrolidinones as potent, broad-spectrum inhibitors of *Leishmania* infection

John A. Kavouris[1,†], **Laura-Isobel McCall**[2,‡], **Miriam A. Giardini**[2], **Geraldine De Muylder**[3,¶], **Diane Thomas**[2], **Adolfo Garcia-Pérez**[4], **Juan Cantizani**[4], **Ignacio Cotillo**[4], **Jose M. Fiandor**[4], **James H. McKerrow**[2,3], **Camila I. De Oliveira**[5], **Jair L. Siqueira-Neto**[§,2,3], **Silvia González**[§,4], **Lauren E. Brown**[§,1], **Scott E. Schaus**[*,§,1]

[1]Department of Chemistry and Center for Molecular Discovery (BU-CMD), Boston University, Boston, Massachusetts, United States of America.

[2]Center for Discovery and Innovation in Parasitic Diseases, Skaggs School of Pharmacy and Pharmaceutical Sciences, University of California San Diego, La Jolla, California, United States of America.

[3]Department of Pathology, Sandler Center for Drug Discovery, University of California San Francisco, San Francisco, California, United States of America.

[4]Global Health Medicines R&D, GlaxoSmithKline, Severo Ochoa 2, 28760 Tres Cantos, Madrid, Spain.

[5]HUPES, Instituto Nacional de Ciência e Tecnologia em Doenças Tropicais (INCT-DT) -Salvador, Brazil; Instituto de Investigação em Imunologia (iii-INCT), São Paulo, Brazil.

Abstract

Introduction: Leishmaniasis is a parasitic disease that affects more than 1 million people worldwide annually, predominantly in resource-limited settings. The challenge in compound development is to exhibit potent activity against the intracellular stage of the parasite (the stage present in the mammalian host) without harming the infected host cells. We have identified a

[*]**Correspondence:** Scott E. Schaus, seschaus@bu.edu.
[†]Present affiliation: Concert Pharmaceuticals, Lexington, Massachusetts, United States of America
[‡]Present affiliation: Department of Chemistry and Biochemistry, Department of Microbiology and Plant Biology, Laboratories of Molecular Anthropology and Microbiome Research, University of Oklahoma, Norman, Oklahoma, United States of America
[¶]Present affiliation: Sciensano, Brussels, Belgium
[§]Equally-contributing senior authors

Author Contributions

J.A.K.: design of experiments, data collection, data analysis and interpretation, writing, editing, revising; L.-I.M. design of experiments, data collection, data analysis and interpretation, editing; M.A.G.: design of experiments, data collection, data analysis and interpretation; G.D.: design of experiments, data collection, data analysis and interpretation, D.T.: data collection, data analysis and interpretation; A.G.-P.: design of experiments, data collection, data analysis and interpretation, writing, editing; J.C.: design of experiments, data collection, data analysis and interpretation, writing, editing; I.C.: design of experiments, data collection, data analysis; J.M.F.: data analysis and interpretation; J.H.M.: design of experiments, data analysis and interpretation; C.I.O.: data analysis and interpretation, writing, editing; J.L.S.-N.: design of experiments, data analysis and interpretation, writing, editing, revising; S.G.: design of experiments, data analysis and interpretation, writing, editing, revising; L.E.B.: design of experiments, data collection, data analysis and interpretation, writing, editing, revising; S.E.S.: design of experiments, data analysis and interpretation, writing, editing, revising. All authors have given approval to the final version of the manuscript.

Supplementary Material

The Supplementary Material (supplementary figures 1–3, supplementary tables S1–S2, and supplementary methods) for this article can be found online at:

Author Manuscript Author Manuscript Author Manuscript Author Manuscript

compound series (pyrazolopyrrolidinones) active against the intracellular parasites of *Leishmania donovani* and *L. major*; the causative agents of visceral and cutaneous leishmaniasis in the Old World, respectively.

Methods: In this study, we performed medicinal chemistry on a newly discovered antileishmanial chemotype, with over 100 analogs tested. Studies included assessments of antileishmanial potency, toxicity towards host cells, and in vitro ADME screening of key drug properties.

Results and discussion: Members of the series showed high potency against the deadliest form, visceral leishmaniasis (approximate $EC_{50} \geq 0.01$ μM without harming the host macrophage up to 10.0 μM). In comparison, the most efficient monotherapy treatment for visceral leishmaniasis is amphotericin B, which presents similar activity in the same assay ($EC_{50} = 0.2$ μM) while being cytotoxic to the host cell at 5.0 μM. Continued development of this compound series with the Discovery Partnership with Academia (DPAc) program at the GlaxoSmithKline Diseases of the Developing World (GSK DDW) laboratories found that the compounds passed all of GSK's criteria to be defined as a potential lead drug series for leishmaniasis.

Conclusion: Here, we describe preliminary structure-activity relationships for antileishmanial pyrazolopyrrolidinones, and our progress towards the identification of candidates for future in vivo assays in models of visceral and cutaneous leishmaniasis.

Keywords

leishmaniasis; heterocycles; pyrazolopyrrolidinone; therapeutics; parasitology; medicinal chemistry; tropical disease; *Leishmania donovani* ; *Leishmania major*

1 Introduction

Leishmaniasis is a disease caused by the *Leishmania* genus of parasites (1) that affects approximately 2 million people worldwide, with 700,000 – 1 million new cases and as many as 50 thousand deaths annually (2). It is the second deadliest parasitic disease after malaria. Leishmaniasis has different clinical manifestations depending on the leishmanial species and patient immune system. Visceral leishmaniasis (VL) is a febrile condition affecting internal organs that can lead to death if left untreated. Historically, first line treatment for VL, predominantly caused by the species *L. donovani* and *L. infantum*/*L. chagasi*, is based on antimonials, a drug formulation using the toxic metal antimony. Second line treatments include IV-administered liposomal amphotericin B (AmBisome, emerging as a first-line treatment in some regions), and miltefosine as an orally administered pill (3). AmBisome is the most effective but prohibitively expensive for the disease population most affected by leishmanial infections. Availability and supply are often a challenge, with the additional requirement that it must be administered in a clinical setting. Miltefosine is teratogenic, toxic to the kidneys and causes gastrointestinal discomfort at the doses necessary to treat the disease, leading to poor compliance in completing a full treatment regimen. Resistance has already become an issue with miltefosine (4, 5), and there are supply challenges due to the public-private partnership model (6).

Cutaneous leishmaniasis (CL) is a generally non-fatal skin condition that produces lesions ultimately leading to permanent scarring and disfigurement. *Leishmania major* causes most

Author Manuscript Author Manuscript Author Manuscript Author Manuscript

CL infections in North Africa, the Middle East, and Central Asia, while *L. braziliensis* and *L. amazonensis* are the leading causative agents of CL in South America. In total, CL infects 1.5 million people worldwide, and the current first line treatment is a pentavalent antimony compound (7) that is delivered by painful intralesional needle injection. Additional challenges in supply, administration, toxicity (8, 9) and resistance (10–12) also make this treatment less than ideal. Advances have been made using topically-administered miltefosine (13), however, there have already been documented failures in this approach due to the rate of parasite mutation (4, 5).

All current approved small-molecule treatments for leishmaniasis are "repurposed" drugs that were developed for other diseases, especially cancer. The current pipeline is underdeveloped (14–18). Drugs for Neglected Diseases (DNDi: www.dndi.org) lists five new compound classes in their clinical antileishmanial portfolio; none have yet progressed beyond Phase I (19). GlaxoSmithKline's lead CRK12 inhibitor GSK3186899 (VL only) (20, 21) completed a Phase I single ascending dose study in 2019, but further clinical evaluation of this compound has been paused following the emergence of non-clinical data for a non-GSK asset with a similar mode-of-action. Oxaborole DNDI-6148 (CL/VL) (14, 15, 22) and nitroimidazole DNDI-0690 (CL/VL) (14, 15, 23–25), have both completed Phase I single ascending dose studies with multiple ascending dose trials underway. Oligo-deoxynucleotide CpG-D35 (CL only) (26–29) and GSK's recently-reported proteasome inhibitor GSK3494245 (30) are also both slated for Phase I study. There remains an unmet clinical need to develop new treatments against leishmaniasis that are ideally inexpensive, readily produced, and orally available as a short course of chemotherapy. Herein, we describe the discovery of a novel antileishmanial compound class, with potent activity against the intracellular stage of the parasite (the most relevant for human disease) in multiple *Leishmania* species.

2 Materials and Methods

2.1 Chemistry

All pyrazolopyrrolidinones were synthesized via a two-step sequence in which pyrrolidinones **4** were first synthesized via Mannich condensation/cyclization of α/γ diketo esters **5** with either pre-isolated or *in situ*-generated imines **6**, followed by Knorr pyrazole condensation with a requisite hydrazine **3** (Figure 1) to produce the desired pyrazolopyrrolidinones. All compounds tested had a purity of >90% as measured by UPLC-MS-ELSD. Full details for compound synthesis and characterization for select pyrazolopyrrolidinones are provided in the Supplementary Information.

2.2 High-throughput screens for antileishmanial compounds at UCSF/UCSD

Compounds were obtained as 0.2 μmoles of dried film for primary single point screening. Each compound was diluted in DMSO to 10 μM final testing concentration. These compounds were tested in 2 biological replicates. The compounds were pre-spotted onto 384-well assay plates in single concentration.

Author Manuscript Author Manuscript Author Manuscript Author Manuscript

Promastigote assay (UCSF)—*Leishmania* promastigotes (*L. major*: strain LV39; *L. donovani*, strain 1S/Cl2D) were maintained as previously described in (31) and (32) at 28 °C in M199 media supplemented with glutamine, adenosine, folic acid, hemin, HEPES, 10% Fetal Bovine Serum (Sigma-Aldrich, cat. no. F2442) and 1% Penicillin-Streptomycin (Gibco, cat. no. 15140122). For the promastigote assay, we followed the method previously described in (33). Briefly, promastigotes were incubated with the compounds for 72 h at 27 °C, then lysed by adding 50 μL of CellTiter-Glo (Promega) and placed on an orbital shaker for 5 min at room temperature. After lysis, the resulting ATP-bioluminescence was measured using the Analyst HT plate reader (Molecular Devices).

Intracellular amastigote assay (UCSF)—THP-1 cells (human acute monocytic leukemia cell line – ATCC TIB202) were grown in RPMI supplemented with 10% Fetal Bovine Serum (FBS) and 50 μM 2-mercaptoethanol at 37 °C in 5% CO_2. THP-1 were seeded in microwell plates at 5×10^5 cells/mL density and treated with 0.1 μM phorbol myristate acetate (PMA, Sigma) at 37 °C for 48 h for differentiation into adherent, non-dividing macrophages. After activation by PMA, cells were washed and incubated with complete RPMI medium containing stationary phase *Leishmania* promastigotes (*L. major:* strain LV39; *L. donovani*, strain 1S/Cl2D) at a 1:15 parasite-cell ratio. Compounds were added and incubated at 37 °C for 72 h. Cells were then washed with phosphate-buffered saline (PBS), fixed for 30 minutes with 4% formaldehyde, rinsed again with PBS, stained for 2 h with 4′,6′-diamidino-2-phenylindole (DAPI 300 nM) and finally washed with PBS (33).

Intracellular amastigote assay (UCSD)—B10R cells (CVCL_0155) were seeded at 300 cells/well, and *L. donovani* WT promastigotes in stationary phase (7th day after passage) were added at 6,000 parasites/well (ratio of 20 parasites/cell). Both cells and parasites were seeded in DMEM High-Glucose medium (Gibco, cat. no. 11995065) containing 5% Fetal Bovine Serum (Sigma-Aldrich, cat. no. F2442) and 1% Penicillin-Streptomycin (Gibco, cat. no. 15140122). Cells and parasites were incubated in the presence of the compounds for 72 h at 37 °C and 5% CO_2. Plates were then fixed with 4% formaldehyde solution for at least 1 h, then washed with 1X PBS and stained with 5 μg/mL DAPI. Plates were read using an ImageXpress microscope (Molecular Devices) and analyzed by MetaXpress software (Molecular Devices) using a custom module optimized for this assay. Compounds that showed relevant antiparasitic activity in the primary screening were retested in serial dilution to obtain a dose-response curve (DRC). Compounds were tested in a 10-point 2-fold serial dilution in 3 technical replicates, and 2 biological replicates. After 72 h, plates were fixed and stained with DAPI as described above. Images were acquired on an ImageXpress microscope, and analyzed using the MetaXpress custom module. The DRCs were plotted, half-effective concentration (EC_{50}) and half-cytotoxic concentration (CC_{50}) were calculated using GraphPad Prism Software, version 6.05 (GraphPad Software, San Diego, CA).

2.3 *In vitro L. donovani* (LD AMMAC) assay at GlaxoSmithKline

The intramacrophage *Leishmania donovani* activity assay (LD AMMAC) at GlaxoSmithKline was performed as described in (34).

Author Manuscript Author Manuscript Author Manuscript Author Manuscript

2.4 Solubility assays

Solubility of compounds using ChemiLuminescent Nitrogen Detection (CLND) was measured as described in (20). Solubility of compounds using Charged Aerosol Detection (CAD) was measured as described in (30). Solubility of solid compounds in Fasted Simulated Intestinal Fluid (FaSSIF) was measured as described in (20, 30).

2.5 Artificial membrane permeability (AMP) assays

Passive permeability of compounds via rate of permeation through an artificial phospholipid membrane at pH 7.4 was measured in a high-throughput format, in duplicate. A solution of 1.8 % phosphatidylcholine in 1% decane was added to a 96-well Millicell filter plate along with 250 μL of 50 mM phosphate buffer, pH 7.4 on the donor side, and 100 μL of the same buffer solution on the receiver side. The assay plate was shaken for 45 minutes before adding test compounds. Test compounds were then added to the filter plate and then incubated at room temperature with shaking for three hours. The donor and receiver solutions were next transferred to a 384-well plate for analysis by LC/MS.

2.6 Microsomal stability assays

Mouse microsomal stability assays were performed as described in (20, 30). Test compounds (0.5 μM) were incubated with female CD1 mouse (Xenotech) liver microsomes and their action started with addition of excess NADPH (8 mg/mL 50 mM potassium phosphate buffer, pH 7.4). Aliquots (50 μL) of the incubation mixture were removed immediately (at time 0) and at 3, 6, 9, 15, and 30 min and mixed with acetonitrile (100 μL) to stop the reaction. Internal standard was added to all samples, the samples were centrifuged to sediment precipitated protein, and the plates were then sealed prior to UPLC-MS/MS analysis using a Quattro Premier XE (Waters Corporation, USA). XLfit (IDBS, UK) was used to calculate the exponential decay and consequently the rate constant (k) from the ratio of the peak area of test compound to internal standard at each time point. The rate of intrinsic clearance (Cl_i) of each test compound was then calculated using the equation Cl_i (mL/min/g liver) = k × V × microsomal protein yield, where V (mL/mg protein) is the incubation volume/mg protein added and microsomal protein yield is taken as 52.5 mg protein/g liver. Verapamil (0.5 μM) was used as a positive control to confirm acceptable assay performance.

2.7 Human serum albumin (HSA) assay

The percentage of compound bound to human serum albumin was measured using a chromatographic method as described in (35, 36). Briefly, each compound was assayed on an immobilized HSA column and gradient retention times measured, with chromatographic peak detection by UV. Each retention time was then converted to a % HSA bound value using a calibration set of compounds with a known % HSA binding.

2.8 Plasma protein binding (PPB) assay

The unbound fraction of compound **1** in plasma was measured using a commercial RED (Rapid Equilibrium Dialysis) plate with inserts (Thermo) with a molecular weight membrane cut off of 8K. The relevant volume of spiked sample matrix was added into the

Author Manuscript Author Manuscript Author Manuscript Author Manuscript

corresponding sample chambers of the RED insert. Three volume equivalents of dialysis buffer were added to the buffer chamber. The dialysis plate was sealed and incubated at 37 °C on a plate shaker for approximately 4 h at 100 rpm. An equivalent volume was removed from each of the three buffer sample chambers and placed into its own well in a clean plate. A specific volume of control matrix was added to each buffer sample for matrix matching. Next, >3X volume of precipitation solvent (acetonitrile + internal standard) was added and the plate was centrifuged. A measured volume of the resulting supernatants was transferred into a clean plate and a specific volume of analytical grade water was added to all samples. Samples were analyzed using a compound-specific LC-MS/MS method to generate analyte peak area ratios which are representative of bound and free drug.

2.9 ChromLogD assay

The chromatographic hydrophobicity index (CHI) values were measured using reversed phase HPLC column (50 mm × 2 mm, 3 μm Gemini NX C18, Phenomenex, U.K.) with fast acetonitrile gradient at starting mobile phase at pH 2, 7.4, and 10.5. CHI values were derived directly from the gradient retention times by using a calibration line obtained for standard compounds. The CHI value approximates to the volume % organic concentration when the compound elutes. CHI was linearly transformed into ChromLogD by least-squares fitting of experimental CHI values to calculated log P (CLogP) values for over 20K research compounds using the following formula: ChromLogD = 0.0857 * $CHI_{7.4}$ − 2.00. The average error of the assay is ± 3 CHI units or ± 0.25 ChromLogD.

2.10 Chiral chromatographic resolution of compound 1

The enantiomers of compound **1** were resolved using semi-preparative chiral HPLC on a Chiralpak IC column (0.46 × 25 cm) using an isocratic mobile phase of 70:30 heptane:ethanol with a 1 mL/min flowrate for 30 minutes. The first- and second-eluding enantiomers of **1** had retention times of 13.9 minutes, and 22.6 minutes, respectively. Independent biological testing of each enantiomer in the LD AMMAC assay indicated that the first-eluting enantiomer (**1a**, T_R=13.9 min) had an EC_{50} of 0.8 μM, and the second-eluting enantiomer (**1b**, T_R = 22.6 min) had an EC_{50} of ~10 μM. The separated enantiomers were next subjected to VCD analysis for absolute stereochemistry assignment as described below.

2.11 VCD analysis of compound 1 enantiomers

A VCD spectrum for each of the separated enantiomers of **1** was obtained in deuterated acetonitrile (~9.8 mg/175 μL concentration) on a BioTools ChiralIR-2X FT-VCD spectrometer operated at 4 cm^{-1}. VCD frequency range was measured from 2400–800 cm^{-1} with PEM calibrated at 1400 cm^{-1} and PEM retardation applied. The first-eluting enantiomer (**1a**) was analyzed using a single two-hour block scan (6240 total scans) and the second-eluting enantiomer (**1b**) was analyzed using the average of six two-hour block scans (37,440 total scans). These experimentally-obtained VCD spectra were utilized in the computational enantiomer assignment as described below.

Author Manuscript Author Manuscript Author Manuscript Author Manuscript

2.12 Computational methods and enantiomer determination

Predicted VCD and IR spectra for the (*R*) enantiomer of compound **1** were generated according to the following computational workflow: first, a conformational search was performed using MOE LowMode algorithm and Amber12:EHT force field with a generalized Born implicit solvent model (dielectric constant = 1). Each unique conformer was then subjected to DFT optimization (B3LYP/DGDZVP2) with VCD vibrational frequency calculation using a polarizable continuum solvent model for acetonitrile. A VCD spectrum was then predicted with fractional populations of each conformer estimated using Boltzmann statistics with a Lorentzian band width of 8 cm^{-1} and a frequency scale factor of 9.9825. This computationally-predicted spectrum was compared to the experimentally obtained spectra using CompareVOA software (BioTools, Inc.) (37) (Supplementary Figure S1). Inspection of the VCD data in the analysis range indicated that the (*R*) model spectrum was largely coincident with that measured on the second-eluting enantiomer **1b**, and was the mirror image of that obtained for the first-eluting enantiomer **1a**. Based on these findings, the bioactive enantiomer **1a** was assigned with (*S*) absolute configuration ((*S*)-**1**), and enantiomer **1b** was assigned with (*R*) absolute configuration ((*R*)-**1**). The confidence limit for these assignments was determined from the absolute values of two parameters in the CompareVOA software: total neighborhood similarity (TNS (VCD)) and the enantiomeric similarity index (ESI)(38). The thresholds for "high" reliability (CL of >99%) are TNS (VCD) ≥ 70 and ESI ≥ 60. In this study, the TNS (VCD) and ESI values were 81.0, and 77.5, respectively, providing an estimated confidence limit of >>99% (very high reliability).

3 Results and Discussion

3.1 High-content screening in *Leishmania* intracellular amastigotes reveals a new antileishmanial pyrazolopyrrolidinone chemotype

In a collaborative effort to identify new antileishmanial chemotypes with minimal host cell cytotoxicity, compounds from the Boston University Center for Molecular Discovery (BU-CMD) screening collection were assessed in a phenotypic, high content primary screen (33) at the University of California's Center for Discovery and Innovation in Parasitic Diseases (CDIPD) for the ability to inhibit growth of *L. donovani* intracellular amastigotes infecting THP-1 cells. From this screen, we identified two pyrazolopyrrolidinones (**1** and **2**, Table 1) which exhibited >99% inhibition of parasite growth with minimal cytotoxicity to the host THP-1 cells (<13% GI). Dose-response testing in *L. donovani* (both intracellular amastigotes and promastigotes) confirmed concentration-dependent growth inhibition of both morphologies of the parasite at low micromolar EC_{50} values for both compounds (Table 1), with host THP-1 cell CC_{50} values >20 μM. Similar activity was subsequently confirmed against both morphologies the cutaneous leishmaniasis-causative species *L. major*, suggestive of broad spectrum antileishmanial activity. Notably, these initial hits had potencies comparable to all existing non-antimonial treatments for the disease (Table 1), as well as to GlaxoSmithKline's current Phase I VL candidates GSK3186899 (intramacrophage EC_{50} = 1.4 μM) and GSK3494245 (intramacrophage EC_{50} = 1.6 μM), which both were chosen for advancement over more potent analogues due to favorable drug properties (e.g. safety, solubility). (21, 30)

Author Manuscript Author Manuscript Author Manuscript Author Manuscript

Compounds **1** and **2** were generated as part of a larger combinatorial library of pyrazolopyrrolidinones (Figure 1, **3**), obtained *via* Knorr pyrazole condensation of 4-acylated 3-hydroxydihydropyrrol-2-ones **4** with hydrazine hydrate. Precursors **4** are easily produced from a Mannich reaction/intramolecular cyclization between α/γ-diketo esters **5** and pre-formed or *in situ*-generated imines **6**. Notably, the three-step reaction sequence is highly robust, and proceeds in high yields on large scales without the need for sophisticated reaction apparatus to exclude air or water ("bucket chemistry"). This feature, combined with the typically inexpensive bulk aldehyde, amine, diketo ester, and hydrazine starting materials, indicate that a future clinical candidate from this compound class could be produced on an industrial scale at low cost. The lack of activity for several near-neighbor analogues in the primary screen provided some nascent SAR (Supplementary Figure 2), hinting at the importance of the *para*-methoxyphenyl moiety at R^1 (vs. phenyl), and the isobutyl group at R^3 (vs. methyl, isopropyl and phenyl).

Based on this preliminary activity profile, we established a collaborative medicinal chemistry project to further evaluate the therapeutic potential of this chemotype at GSK's Tres Cantos Open Lab Foundation (TCOLF) site under the auspices of GSK's Discovery Partnership in Academia (DPAc) Program. At the outset of the DPAc collaborative project, compound **1** was evaluated against GSK's established criteria for antileishmanial compound advancement (Table 2). Some of these assessments were performed on racemic **1**, while we also pursued chiral separation of the **1** racemate to determine the active enantiomer. Preparative chiral-SFC was used to separate enantioenriched **1** on a multigram scale, and vibrational circular dichroism (VCD) analysis confirmed the absolute (*S*)-stereochemistry of the active enantiomer (Figure 2, Supplementary Figure 1), which had an improved EC_{50} of 0.8 μM. As shown in Table 2, compound **1** performed well against most of GSK's lead selection criteria, and met minimum standards toward advancement as a lead compound, with a few criteria accepted despite not falling within ideal ranges: human serum albumin binding and property forecast index (PFI), a hydrophobicity metric developed at GSK which considers lipophilicity and aromatic ring count and is predictive of downstream developability (39, 40). Based on this promising profile, we progressed into medicinal chemistry optimization to better understand structure-activity relationships (SAR) toward improved potency, as well as structure-property relationships (SPR) with an eye toward reducing PFI and plasma protein binding.

3.2 Medicinal chemistry of pyrazolopyrrolidinones establishing preliminary structure-activity and structure-property relationships toward improved leads

The pyrazolopyrrolidinone chemotype is well-described in the research and patent literature, with a rich array of reported biological activities, the most prominent of which are p53/MDM2 interaction inhibition (41–49), phosphodiesterase inhibition (50, 51), and GPR55 modulation (52–56). In addition, there are examples of pyrazolopyrrolidinones exhibiting P2X3 antagonism (57), GPR68 agonism (58), 5-HT1A receptor binding, (59) BET inhibition (60, 61), 14-3-3-PMA2 interaction stabilization (62), P-glycoprotein inhibition (63), antitumor activity (64), and antimicrobial activity against various parasitic, viral and bacterial species including *T. cruzi* (65), HIV (66, 67), flaviviruses (68), *M. tuberculosis* (69, 70), *P. falciparum* (71, 72), and *V. cholerae* (73). Interestingly, most of the aforementioned

Author Manuscript Author Manuscript Author Manuscript Author Manuscript

activities are relegated to pyrazolopyrrolidinones wherein R^3 is an aryl substituent. This phenomenon may, however, be attributable to the ease of synthesis of such compounds and their precursors. An important exception to the R^3 arylation trend is observed among select inhibitors of the p53/MDM2 interaction. In all of these inhibitors, the R^1/R^2 diarylated motif has been shown crystallographically to be a critical binding element at the Leu26 and Trp23 subpockets of MDM2, a similar pharmacophore and binding mode to that exhibited by other diarylated p53/MDM2 inhibitors such as nutlin. Among these inhibitors, non-aryl R^3 substitutions such as methyl, isopropyl, and *tert*-butyl have all been shown to confer some degree of inhibition (47). Other scattered exceptions include a class of purinoreceptor antagonists with similarly broad tolerance for R^3 substitution (74), and two examples of R^3-methyl substituted inhibitor chemotypes: EPX-107979, annotated as a folding corrector of F508del-CFTR (75) and 11β-hydroxysteroid dehydrogenase inhibitors ZINC01292412 and ZINC01260941 (76). Importantly, however, there are no reported examples to-date of pyrazolopyrrolidinones bearing the R^3 = ^{i}Bu substitution, which from our primary screen SAR (Supplementary Figure 2) appeared to be critical for antileishmanial activity in the absence of host toxicity. While the target of antileishmanial pyrazolopyrrolidinones has yet to be defined, and we cannot conclusively rule out any of the aforementioned targets as being implicated in this activity, the consistent lack of antileishmanial activity among the many R^3 phenyl-, isopropyl- and methyl-substituted pyrazolopyrrolidinones tested in the primary screen is suggestive of a target for the R^3 isobutylated compounds which is orthogonal to those already appearing in the vast pyrazolopyrrolidinone literature.

Concurrent with the evaluation of screening hit **1** against GSK TCOLF's lead advancement criteria (Table 2), we executed a preliminary medicinal chemistry campaign to improve our understanding of structure-activity relationships (SAR) for this series, to target compounds with improved potencies and physicochemical properties to potentially supersede compound **1** as an advanced lead.

Given the literature precedents described above and the apparent narrow tolerance for R^3 substitutions observed in the primary screen compounds, we first undertook a thorough and methodical assessment of tolerated groups at the three points of diversity ($R^1/R^2/R^3$) for the core. At this stage of the project, all analogues were assessed using a battery of assays performed in-house at GlaxoSmithKline. For antileishmanial activity, we utilized GSK's inMac assay (77). This assay provides two readouts of compound potency: average number of intracellular amastigotes per infected cell (AMMAC) EC_{50}, percentage of infected cells per well (INFCELL) EC_{50}, as well as a toxicity output derived from the number of host cells (MAC EC_{50}). In addition, compounds were assessed for toxicity against HepG2 cells (HEPG2 EC_{50}). Here, we focus on AMMAC EC_{50} values for relative potency assessments. Using this data, we calculated a selectivity index (SI) for each compound, described here as a macrophage SI (SI MAC), using the equation SI MAC = (MAC EC_{50})/(AMMAC EC_{50}). It should be noted that for all compounds assessed in this project, the measured toxicity against THP-1 macrophages either equaled or exceeded that of HepG2 hepatocytes, therefore the SI MAC is used here as the more conservative estimate of therapeutic index.

Revisiting the initial profile of compound **1** against GSK's lead selection criteria, we identified a number of properties requiring improvement, including PFI, plasma protein

Author Manuscript Author Manuscript Author Manuscript Author Manuscript

binding, and a larger SI relative to THP-1 and HepG2 cells. While the CLND solubility fell below the ideal range, good FaSSIF solubility suggested viability as an orally available drug. We used the potency and physiochemical data for **1** as a benchmark for guidance as we began investigating the SAR to identify an improved lead compound for series progression and advancement to animal studies. In these studies, human serum albumin (HSA) binding was employed as a surrogate for plasma protein binding.

Starting first at R^3, we explored a variety of aliphatic substitutions, determining that some branched aliphatics of similar size to the parent isobutyl (e.g. isopentyl/neopentyl, Table 3, compounds **9**-**10**) exhibited comparable potencies and low host cell toxicities, whereas the linear *n*-butyl (compound **11**) showed a significant increase in potency (~300 nM) that was accompanied by a toxicity increase to the low micromolar range (2.5 μM). Similar effects were observed with *n*-but-1-ene and 2-methyl-*n*-but-1-ene substitutions (compounds **12**-**13**). Finally, surveys of additional branched aliphatic (**13**) and aromatic (compounds **14**-**17**) substituents at R^3 failed to produce more potent compounds than **1**, and often showed significant decreases in selectivity index. While the isopentyl/neopentyl analogues **9** and **10** showed marginal improvements over **1** with respect to their macrophage toxicity, these improvements were offset by equivalently small increases in HepG2 toxicity and significant reductions in solubility/permeability; as such we opted to retain the R^3 isobutyl substituent in all future analogues.

We next examined the effects of modifying the R^1 *para*-methoxyphenyl substituent (Table 4). Direct conversion of the methyl ether to phenol (compound **18**) suppressed both antileishmanial activity and toxicity. The ethyl ether analogue **19** exhibited modest improvements in both activity and toxicity as compared to the parent methyl, while the trifluoromethoxy ether (**20**) ablated antileishmanial activity to levels below that of the inherent THP1-cell toxicity. The dimethylamino analogue **21** showed significantly improved potency and selectivity index, while the ethyl-, fluoro-, bromo-, *tert*-butyl- and methyl ester-substituted analogues (compounds **22**-**25**) had comparable activities and therapeutic indices to **1**. In contrast to methyl ester **26**, hydrolyzed carboxylic acid **27** was inactive. Lastly, replacement of the *para*-methoxy with an *N*-linked imidazole (compound **28**) afforded an equipotent compound with reduced cytotoxicity, leading to an improved SI. However, all improvements in potency (**24**, **26**) or host cell toxicity (**26**, **28**) leading to improved selectivity index were accompanied by significant reductions CLND solubility.

Next, we examined alternate substitution patterns on the R^1 aryl ring (Table 5). Movement of the methoxy group from *para*- to the *ortho*- (**29**) or *meta*-positions (**30**) ablated activity, as did nitrogenation of the ring in the presence (**31**) or absence (**32**-**33**) of the *para*-methoxy group. Additional unsuccessful modifications explored included homologation of the *para*-methoxyphenyl moiety to a *para*-methoxybenzyl (**34**), and additional furyl (**35**) and non-aromatic substituents (**36**-**41**); although several of these modifications led to significant improvements in key properties such as reduced host cell toxicity, and improved solubility, permeability, HSA binding, and PFI, none were able to achieve inhibition of parasite replication below 10 μM EC_{50} values.

Author Manuscript Author Manuscript Author Manuscript Author Manuscript

In contrast, we found more success in replacing the *para*-methoxyphenyl group with disubstituted benzene and bicyclic heteroaromatic substituents (Table 6). For example, *meta*-fluorination of **1** (**42**) led to modest increases in both potency and selectivity, albeit with the reduction in solubility as would be expected due to the increased lipophilicity. In contrast, addition of an *ortho*-methoxy substituent to **1** (**43**) improved solubility, again at the expense of activity. The replacement of the methoxy moiety with various 3,4-fused heterocycles (methylenedioxy **44**, ethylenedioxy **45**, and triazolopyridine **46**) all led to modest improvements in selectivity via reduced host cell toxicity. However, none of these analogues showed improved solubility relative to **1** despite the presence of additional heteroatoms, which was apparently offset by the increased planarity imparted by the bicyclic systems.

With an improved understanding of R^1 and R^3 SAR, we next advanced to modifications of R^2 (Table 7), where our initial screening SAR indicated that deletion of the *para*-fluoro substituent (compound **2**) afforded a similarly potent compound to **1**, whereas replacement of the fluorine with a methyl group resulted in 0% inhibition at 10 μM (**CMLD007430**, Supplementary Figure 2). Consistent with this, our efforts to replace the fluorine with other halogens (**47**-**48**), trifluoromethyl (**49**), carboxylate (**50**) and methyl carboxylate (**51**) substituents all reduced potency, as did replacement of the phenyl ring with cyclohexyl and cyclopentyl moieties (compounds **52**-**53**). Interestingly, improved potencies and selectivity indexes were achieved with several types of *ortho*-substituents, including halogens (**54**-**56**) and a methyl ether (**57**), whereas none such improvements were observed with the equivalent *meta*-substituents (**58**-**62**). Consistent with this trend, addition of *ortho*-substituents to the *para*-fluorinated **1** (**63**-**64**) led to improved potency, whereas addition of a *meta*-fluoro to the same scaffold did not (**65**). Lastly, 2,6-dichloro substitution of the R^2 phenyl ring (compound **66**) led to improved potency but with a considerable increase in host cell toxicity.

In an effort to improve solubility *via* R^2 modifications, we also surveyed a diverse array of substituted and unsubstituted heteroaromatic groups at this position (Supplementary Table S1). While several of these compounds exhibited the expected improvements in CLND solubility and reduction in HSA binding, potency was also significantly compromised for this set.

With the scope and limitations of R^1/R^2 substitutions mapped with respect to potency and property improvements, we next attempted to pair promising groups at each site to arrive at optimized new inhibitors. Based on the trends observed in the initial series, it was clear that improvements in solubility and reduced human serum albumin binding would require reduced lipophilicity (CLogP), a modification which generally also correlated with reduced potency in our initial analogues. To offset this, we focused on reducing global LogP *via* modifications to R^1 (where increased polarity appeared to be more tolerable), in combination with the apparent potency-enhancing *ortho*-substituents at R^2. Table 8 depicts the most successful of these pairings with respect to potency, selectivity, HSA binding, and solubility. Of note, at this later stage in the project solubility was measured using charged aerosol detection (CAD), due to a change in standard *in vitro* ADME methods employed at GSK. In addition, infection EC_{50} and host cell CC_{50} measurements were obtained in

Author Manuscript Author Manuscript Author Manuscript Author Manuscript

a comparable *L. donovani* infection model performed at the University of California, San Diego (see Methods). In order to benchmark compound performance across the two assays, a random sampling of compounds was selected for re-assessment in the UCSD infection assay (Supplementary Table S2). Most compounds showed slightly improved potency in the UCSD assay than was observed in the LD AMMAC assay run at GSK; as a representative example, the UCSD potency for racemic **1** was found to be 0.82 μM (Table 8, entry 1), compared to 2.5 μM in the GSK LD AMMAC assay. Despite the change in absolute potency values, the two assays were well-correlated with respect to relative potencies, with a Pearson's correlation coefficient of 0.74. (Supplementary Table S2 and Supplementary Figure 3).

From this compound series, the *ortho*-substituted R^2 groups (B1-B4) significantly improved potency and selectivity, even when paired with groups at R^1 which had conferred reduced potency when paired with the R^2 *para*-fluorophenyl moiety (e.g. A4/A5, Compounds **78**-**87**). Several inhibitors in this series, **69**, **86** and **87**, exhibited the desired improvements across all key physicochemical properties, in addition to improved potency and selectivity. However, for a large proportion of these compounds the most significant gains in potency were offset by an increase in toxicity, PFI and HSA binding, and a reduction in solubility owing to increased lipophilicity. Efforts to optimize from **69**, **86** and **87** toward further improved analogues are ongoing in our laboratory. Importantly, like compound **1**, pyrazolopyrrolidinone compounds **69**, **86** and **87**, are inexpensive to produce on scale and show limited host cell cytotoxicity relative to their antiparasitic activity. These features underscore the potential for pyrazolopyrrolidinones to significantly improve the current state-of-the-art for controlling leishmaniasis, where the limited arsenal of existing first-line treatments are expensive (e.g. amphotericin) or toxic (e.g. miltefosine).

4 Conclusion

In this study, we discovered a novel antileishmanial pyrazolopyrrolidinone chemotype that is effective against the intracellular amastigote parasite morphology in multiple *Leishmania* species with minimal host cytotoxicity. Compared to all of the advanced leads in the current antileishmanial pipeline, pyrazolopyrrolidinones are extremely facile to produce, without the need for sophisticated reaction apparatus in two synthetic steps from low-cost commodity starting materials – an ideal attribute for a therapeutic targeting a neglected tropical disease. Subsequent medicinal chemistry optimization has produced multiple advanced leads with significantly improved potency and ADME parameters relative to the initial hit, and support further preclinical optimization of the series. Work to advance these and similar candidates into *in vivo* pharmacokinetic and efficacy assessments is ongoing.

Supplementary Material

Refer to Web version on PubMed Central for supplementary material.

Author Manuscript Author Manuscript Author Manuscript Author Manuscript

Acknowledgments

In vitro experiments at UC San Diego were conducted in the UCSD Screening Core. We are grateful to the National Science Foundation for the purchase of the Waters high resolution mass spectrometer (CHE 0443618) used in this work. B10R cells were provided by Martin Olivier, McGill University.

Funding

This work was supported by a Discovery Partnerships in Academia (DPAc) Award from GlaxoSmithKline (to J.A.K., L.E.B., S.E.S.) and a grant from the National Institutes of Health (Grant R01AI151639 to C.I.O., J.L.S.-N., L.E.B., and S.E.S.).

Conflict of Interest

The authors declare the following competing financial interest(s):

J.A.K., J.H.M., G.D., C.I.O., J.L.S.-N., L.E.B., and S.E.S. are named as inventors on a patent application pertaining to findings reported here. A.G.-P., J.C., I.C., and S.G. are employed by GlaxoSmithKline. J.F. was formerly employed by GlaxoSmithKline. This study received funding from GlaxoSmithKline. GlaxoSmithKline had the following involvement in the study: design of experiments, data collection, data analysis and interpretation, writing, editing and revising.

References

1. Ashford RW, Bern C, Boelaert M, Bryceson A, Chappuis F, Croft S, et al. (2010). Control of the Leishmaniases: Report of a Meeting of the WHO Expert Committee on the Control of Leishmaniases. Geneva, Switzerland: World Health Organization.
2. Vos T, Allen C, Arora M, Barber RM, Bhutta ZA, Brown A, et al. Global, Regional, and National Incidence, Prevalence, and Years Lived with Disability for 310 Diseases and Injuries, 1990–2015: A Systematic Analysis for the Global Burden of Disease Study 2015. The Lancet (2016) 388(10053):1545–602. doi: 10.1016/s0140-6736(16)31678-6.
3. Vakil NH, Fujinami N, Shah PJ. Pharmacotherapy for Leishmaniasis in the United States: Focus on Miltefosine. Pharmacotherapy (2015) 35(5):536–45. doi: 10.1002/phar.1585. [PubMed: 25940658]
4. Srivastava S, Mishra J, Gupta AK, Singh A, Shankar P, Singh S. Laboratory Confirmed Miltefosine Resistant Cases of Visceral Leishmaniasis from India. Parasit Vectors (2017) 10(1):49. doi: 10.1186/s13071-017-1969-z. [PubMed: 28137296]
5. Bhattacharya A, Ouellette M. New Insights with Miltefosine Unresponsiveness in Brazilian *Leishmania infantum* Isolates. EBioMedicine (2018) 37:13–4. doi: 10.1016/j.ebiom.2018.10.016. [PubMed: 30314891]
6. Sunyoto T, Potet J, Boelaert M. Why Miltefosine-a Life-Saving Drug for Leishmaniasis-Is Unavailable to People Who Need It the Most. BMJ Glob Health (2018) 3(3):e000709 doi: 10.1136/bmjgh-2018-000709.
7. Frezard F, Demicheli C, Ribeiro RR. Pentavalent Antimonials: New Perspectives for Old Drugs. Molecules (2009) 14(7):2317–36. doi: 10.3390/molecules14072317. [PubMed: 19633606]
8. Sundar S, Sinha PR, Agrawal NK, Srivastava R, Rainey PM, Berman JD, et al. A Cluster of Cases of Severe Cardiotoxicity among Kala-Azar Patients Treated with a High-Osmolarity Lot of Sodium Antimony Gluconate. Am J Trop Med Hyg (1998) 59(1):139–43. doi: 10.4269/ajtmh.1998.59.139. [PubMed: 9684642]
9. Sundar S, Chakravarty J. Antimony Toxicity. Int J Environ Res Public Health (2010) 7(12):4267–77. doi: 10.3390/ijerph7124267. [PubMed: 21318007]
10. Ait-Oudhia K, Gazanion E, Vergnes B, Oury B, Sereno D. Leishmania Antimony Resistance: What We Know What We Can Learn from the Field. Parasitol Res (2011) 109(5):1225–32. doi: 10.1007/s00436-011-2555-5. [PubMed: 21800124]
11. Jha RK, Sah AK, Shah DK, Sah P. The Treatment of Visceral Leishmaniasis: Safety and Efficacy. JNMA J Nepal Med Assoc (2013) 52(192):645–51. doi: 10.31729/jnma.2444 [PubMed: 25327244]

Author Manuscript Author Manuscript Author Manuscript Author Manuscript

12. Vieira-Goncalves R, Fagundes-Silva GA, Heringer JF, Fantinatti M, Da-Cruz AM, Oliveira-Neto MP, et al. First Report of Treatment Failure in a Patient with Cutaneous Leishmaniasis Infected by *Leishmania* (*Viannia*) Naiffi Carrying *Leishmania* RNA Virus: A Fortuitous Combination? Rev Soc Bras Med Trop (2019) 52:e20180323. doi: 10.1590/0037-8682-0323-2018. [PubMed: 30994803]
13. Tahir M, Bashir U, Hafeez J, Ghafoor R. Safety and Efficacy of Miltefosine in Cutaneous Leishmaniasis: An Open Label, Non-Comparative Study from Balochistan. Pak J Med Sci (2019) 35(2):495–9. doi: 10.12669/pjms.35.2.54. [PubMed: 31086539]
14. Van Bocxlaer K, Caridha D, Black C, Vesely B, Leed S, Sciotti RJ, et al. Novel benzoxaborole, nitroimidazole and aminopyrazoles with activity against experimental cutaneous leishmaniasis. Int J Parasitol Drugs Drug Resist (2019) 11:129–38. doi: 10.1016/j.ijpddr.2019.02.002 [PubMed: 30922847]
15. Van den Kerkhof M, Mabille D, Chatelain E, Mowbray CE, Braillard S, Hendrickx S, et al. *In Vitro* and *in Vivo* Pharmacodynamics of Three Novel Antileishmanial Lead Series. Int J Parasitol Drugs Drug Resist (2018) 8(1):81–6. doi: 10.1016/j.ijpddr.2018.01.006. [PubMed: 29425734]
16. Singh N, Kumar M, Singh RK. Leishmaniasis: Current Status of Available Drugs and New Potential Drug Targets. Asian Pac J Trop Med (2012) 5(6):485–97. doi: 10.1016/s1995-7645(12)60084-4. [PubMed: 22575984]
17. Sundar S, Singh A. Chemotherapeutics of Visceral Leishmaniasis: Present and Future Developments. Parasitology (2018) 145(4):481–9. doi: 10.1017/s0031182017002116. [PubMed: 29215329]
18. Health Products in the Pipeline for Infectious Diseases: World Health Organization (2018). URL: https://www.who.int/observatories/global-observatory-on-health-research-and-development/monitoring/health-products-in-the-pipeline-for-infectious-diseases-Jan-18 (Accessed 2022 Dec 2).
19. Portfolio - DNDI: Drugs for Neglected Diseases Initiative (2019) [cited 2019 June 5]. Available from: https://www.dndi.org/diseases-projects/leishmaniasis/leish-portfolio/.
20. Thomas MG, De Rycker M, Ajakane M, Albrecht S, Alvarez-Pedraglio AI, Boesche M, et al. Identification of Gsk3186899/Ddd853651 as a Preclinical Development Candidate for the Treatment of Visceral Leishmaniasis. J Med Chem (2019) 62(3):1180–202. doi: 10.1021/acs.jmedchem.8b01218. [PubMed: 30570265]
21. Wyllie S, Thomas M, Patterson S, Crouch S, De Rycker M, Lowe R, et al. Cyclin-Dependent Kinase 12 Is a Drug Target for Visceral Leishmaniasis. Nature (2018) 560(7717):192–7. doi: 10.1038/s41586-018-0356-z. [PubMed: 30046105]
22. Jacobs RT, Plattner JJ, Keenan M. Boron-Based Drugs as Antiprotozoals. Curr Opin Infect Dis (2011) 24(6):586–92. doi: 10.1097/QCO.0b013e32834c630e. [PubMed: 22001943]
23. Thompson AM, O'Connor PD, Blaser A, Yardley V, Maes L, Gupta S, et al. Repositioning Antitubercular 6-Nitro-2,3-Dihydroimidazo[2,1-*b*][1,3]Oxazoles for Neglected Tropical Diseases: Structure-Activity Studies on a Preclinical Candidate for Visceral Leishmaniasis. J Med Chem (2016) 59(6):2530–50. doi: 10.1021/acs.jmedchem.5b01699. [PubMed: 26901446]
24. Thompson AM, O'Connor PD, Marshall AJ, Blaser A, Yardley V, Maes L, et al. Development of (6R)-2-Nitro-6-[4-(Trifluoromethoxy)Phenoxy]-6,7-Dihydro-5H-Imidazo[2,1- *b*][1,3]Oxazine (DNDI-8219): A New Lead for Visceral Leishmaniasis. J Med Chem (2018) 61(6):2329–52. doi: 10.1021/acs.jmedchem.7b01581. [PubMed: 29461823]
25. Thompson AM, O'Connor PD, Marshall AJ, Yardley V, Maes L, Gupta S, et al. 7-Substituted 2-Nitro-5,6-Dihydroimidazo[2,1-*b*][1,3]Oxazines: Novel Antitubercular Agents Lead to a New Preclinical Candidate for Visceral Leishmaniasis. J Med Chem (2017) 60(10):4212–33. doi: 10.1021/acs.jmedchem.7b00034. [PubMed: 28459575]
26. Flynn B, Wang V, Sacks DL, Seder RA, Verthelyi D. Prevention and Treatment of Cutaneous Leishmaniasis in Primates by Using Synthetic Type D/A Oligodeoxynucleotides Expressing CpG Motifs. Infect Immun (2005) 73(8):4948–54. doi: 10.1128/IAI.73.8.4948-4954.2005. [PubMed: 16041009]
27. Verthelyi D, Gursel M, Kenney RT, Lifson JD, Liu S, Mican J, et al. Cpg Oligodeoxynucleotides Protect Normal and SIV-Infected Macaques from *Leishmania* Infection. J Immunol (2003) 170(9):4717–23. doi: 10.4049/jimmunol.170.9.4717. [PubMed: 12707351]

Author Manuscript Author Manuscript Author Manuscript Author Manuscript

28. Walker PS, Scharton-Kersten T, Krieg AM, Love-Homan L, Rowton ED, Udey MC, et al. Immunostimulatory Oligodeoxynucleotides Promote Protective Immunity and Provide Systemic Therapy for Leishmaniasis Via IL-12- and IFN-Gamma-Dependent Mechanisms. Proc Natl Acad Sci USA (1999) 96(12):6970–5. doi: 10.1073/pnas.96.12.6970. [PubMed: 10359823]
29. Zimmermann S, Egeter O, Hausmann S, Lipford GB, Rocken M, Wagner H, et al. Cutting Edge: CpG Oligodeoxynucleotides Trigger Protective and Curative Th1 Responses in Lethal Murine Leishmaniasis. J Immunol (1998) 160(8):3627–30. [PubMed: 9558060]
30. Wyllie S, Brand S, Thomas M, De Rycker M, Chung CW, Pena I, et al. Preclinical Candidate for the Treatment of Visceral Leishmaniasis That Acts through Proteasome Inhibition. Proc Natl Acad Sci USA (2019) 116(19):9318–23. doi: 10.1073/pnas.1820175116. [PubMed: 30962368]
31. McCall LI, El Aroussi A, Choi JY, Vieira DF, De Muylder G, Johnston JB, et al. Targeting Ergosterol Biosynthesis in *Leishmania donovani*: Essentiality of Sterol 14 Alpha-Demethylase. PLoS Negl Trop Dis (2015) 9(3):e0003588. doi: 10.1371/journal.pntd.0003588. [PubMed: 25768284]
32. Parab AR, Thomas D, Lostracco-Johnson S, Siqueira-Neto JL, McKerrow JH, Dorrestein PC, et al. Dysregulation of glycerophosphocholines in the cutaneous lesion caused by *Leishmania major* in experimental murine models. Pathogens (2021) 10(5):593. doi: 10.3390/pathogens10050593 [PubMed: 34068119]
33. De Muylder G, Ang KKH, Chen S, Arkin MR, Engel JC, McKerrow JH. A Screen against *Leishmania* Intracellular Amastigotes: Comparison to a Promastigote Screen and Identification of a Host Cell-Specific Hit. PLoS Negl Trop Dis (2011) 5(7):e1253. doi: 10.1371/journal.pntd.0001253. [PubMed: 21811648]
34. De Rycker M, Hallyburton I, Thomas J, Campbell L, Wyllie S, Joshi D, et al. Comparison of a High-Throughput High-Content Intracellular *Leishmania donovani* Assay with an Axenic Amastigote Assay. Antimicrob Agents Chemother (2013) 57(7):2913–22. doi: 10.1128/AAC.02398-12. [PubMed: 23571538]
35. Valko K, Nunhuck S, Bevan C, Abraham MH, Reynolds DP. Fast Gradient HPLC Method to Determine Compounds Binding to Human Serum Albumin. Relationships with Octanol/Water and Immobilized Artificial Membrane Lipophilicity. J Pharm Sci (2003) 92(11):2236–48. doi: 10.1002/jps.10494. [PubMed: 14603509]
36. Bunally S, Young RJ. The Role and Impact of High Throughput Biomimetic Measurements in Drug Discovery. ADMET and DMPK (2018) 6(2):74–84. doi: 10.5599/admet.530.
37. Debie E, Bultinck P, Nafie L, Dukor R. CompareVOA. Jupiter, FL: BioTools, Inc. (2010).
38. Debie E, De Gussem E, Dukor RK, Herrebout W, Nafie LA, Bultinck P. A Confidence Level Algorithm for the Determination of Absolute Configuration Using Vibrational Circular Dichroism or Raman Optical Activity. ChemPhysChem (2011) 12(8):1542–9. doi: 10.1002/cphc.201100050. [PubMed: 21542094]
39. Leeson PD, Young RJ. Molecular Property Design: Does Everyone Get It? ACS Med Chem Lett (2015) 6(7):722–5. doi: 10.1021/acsmedchemlett.5b00157. [PubMed: 26191353]
40. Young RJ, Green DV, Luscombe CN, Hill AP. Getting Physical in Drug Discovery II: The Impact of Chromatographic Hydrophobicity Measurements and Aromaticity. Drug Discov Today (2011) 16(17–18):822–30. doi: 10.1016/j.drudis.2011.06.001. [PubMed: 21704184]
41. Furet P, Guagnano V, Holzer P, Kallen J, Mah R, Masuya K, et al. (2015). Pyrazolo[3,4-*d*]Pyrimidinone Compounds as Inhibitors of the p53/MDM2 Interaction. U.S. Patent No 2015/0353563 A1 Washington, DC: U.S. Patent and Trademark Office.
42. Furet P, Guagnano V, Holzer P, Kallen J, Mah R, Masuya K, et al. (2014). Preparation of Pyrazolo[3,4-*d*]Pyrimidinone Compounds as Inhibitors of the p53/MDM2 Interaction. International Patent No WO 2014/115080 A1. Geneva, Switzerland: World Intellectual Property Organization.
43. Furet P, Guagnano V, Holzer P, Mah R, Masuya K, Schlapbach A, et al. (2013) Preparation of Pyrazolopyrrolidine Compounds as Modulators of MDM2 and MDM4 for Therapy. International Patent No WO 2013/080141 A1. Geneva, Switzerland: World Intellectual Property Organization.
44. Furet P, Masuya K, Kallen J, Stachyra-Valat T, Ruetz S, Guagnano V, et al. Discovery of a Novel Class of Highly Potent Inhibitors of the p53-MDM2 Interaction by Structure-Based Design

Author Manuscript Author Manuscript Author Manuscript Author Manuscript

Starting from a Conformational Argument. Bioorg Med Chem Lett (2016) 26(19):4837–41. doi: 10.1016/j.bmcl.2016.08.010. [PubMed: 27542305]

45. Zhou W-H, Xu X-G, Li J, Min X, Yao J-Z, Dong G-Q, et al. Design, Synthesis and Structure-Activity Relationship of 4,5-Dihydropyrrolo[3,4-*c*]Pyrazol-6(1*H*)-Ones as Potent p53-MDM2 Inhibitors. Chin Chem Lett (2017) 28(2):422–5. doi: 10.1016/j.cclet.2016.09.001.
46. Zhuang C, Miao Z, Wu Y, Guo Z, Li J, Yao J, et al. Double-Edged Swords as Cancer Therapeutics: Novel, Orally Active, Small Molecules Simultaneously Inhibit P53-Mdm2 Interaction and the NF-kB Pathway. J Med Chem (2014) 57(3):567–77. doi: 10.1021/jm401800k. [PubMed: 24428757]
47. Kallen J, Izaac A, Chau S, Wirth E, Schoepfer J, Mah R, et al. Structural States of Hdm2 and HdmX: X-Ray Elucidation of Adaptations and Binding Interactions for Different Chemical Compound Classes. ChemMedChem (2019) 14(14):1305–14. doi: 10.1002/cmdc.201900201. [PubMed: 31066983]
48. Lopez-Dominguez JA, Laberge R-M, Campisi J, Davalos A, Demaria M, David N, et al. (2017) Compositions and Methods for Treating Senescence-Associated Diseases and Disorders. International Patent No WO 2017/008060 A1. Geneva, Switzerland: World Intellectual Property Organization.
49. Tortorella P, Laghezza A, Durante M, Gomez-Monterrey I, Bertamino A, Campiglia P, et al. An Effective Virtual Screening Protocol to Identify Promising p53-MDM2 Inhibitors. J Chem Inf Model (2016) 56(6):1216–27. doi: 10.1021/acs.jcim.5b00747. [PubMed: 27269808]
50. Duplantier AJ. (1995) Preparation of 4,6-Dihydro-1*H*-Pyrazolo[3,4-*c*]Pyrrole Inhibitors of Phosphodiesterase IV and Tumor Necrosis Factor. International Patent No WO 95/19362 A1. Geneva, Switzerland: World Intellectual Property Organization.
51. Gomez Bateman S, Jurkiewicz I, Hermann GJ, Matthews ITW, Kirby JP, Lopez EH, et al. (2012) Pyrrolopyrazolones as Phosphodiesterase Inhibitors and Their Preparation and Their Use in the Treatment of Viral Infection and Oncological Diseases. International Patent No WO 2012/046030 A2. Geneva, Switzerland: World Intellectual Property Organization.
52. Brown AJ, Castellano-Pellicena I, Haslam CP, Nichols PL, Dowell SJ. Structure-Activity Relationship of the Gpr55 Antagonist, CID16020046. Pharmacology (2018) 102(5–6):324–31. doi: 10.1159/000493490. [PubMed: 30296786]
53. Zeng Y, Liu Z, Tan X, Lei L. The Gpr55 Antagonist CID16020046 Mitigates Advanced Glycation End Products (AGEs) Induced Chondrocyte Activation. Chem-Biol Interact (2020) 325:109088. doi: 10.1016/j.cbi.2020.109088. [PubMed: 32360554]
54. Wang Y, Pan W, Wang Y, Yin Y. The Gpr55 Antagonist CID16020046 Protects against Ox-LDL-Induced Inflammation in Human Aortic Endothelial Cells (Haecs). Arch Biochem Biophys (2020) 681:108254. doi: 10.1016/j.abb.2020.108254. [PubMed: 31904362]
55. Kargl J, Brown AJ, Andersen L, Dorn G, Schicho R, Waldhoer M, et al. A Selective Antagonist Reveals a Potential Role of G Protein-Coupled Receptor 55 in Platelet and Endothelial Cell Function. Journal of Pharmacology and Experimental Therapeutics (2013) 346(1):54–66. doi: 10.1124/jpet.113.204180. [PubMed: 23639801]
56. Hampe J, Thangapandi R, Brosch M, Schafmeyer C. (2019). Medicament for the Treatment of Liver Fibrosis and Cirrhosis of Liver Comprising an Inhibitor of Gpr55. International Patent No WO 2019/121764 A1. Geneva, Switzerland: World Intellectual Property Organization.
57. Tobinaga H, Kameyama T, Asahi K, Horiguchi T, Oohara M, Taoda Y, et al. Pyrrolinone Derivatives as a New Class of P2X3 Receptor Antagonists. Part 3: Structure-Activity Relationships of Pyrropyrazolone Derivatives. Bioorg Med Chem Lett (2020) 30(24):127636. doi: 10.1016/j.bmcl.2020.127636. [PubMed: 33132115]
58. Huang X-P, Karpiak J, Kroeze WK, Zhu H, Chen X, Moy SS, et al. Allosteric Ligands for the Pharmacologically Dark Receptors Gpr68 and Gpr65. Nature (2015) 527(7579):477–83. doi: 10.1038/nature15699. [PubMed: 26550826]
59. Warszycki D, Rueda M, Mordalski S, Kristiansen K, Satala G, Rataj K, et al. From Homology Models to a Set of Predictive Binding Pockets-a 5-HT1a Receptor Case Study. J Chem Inf Model (2017) 57(2):311–21. doi: 10.1021/acs.jcim.6b00263. [PubMed: 28055203]

Author Manuscript Author Manuscript Author Manuscript Author Manuscript

60. Blank J, Bordas V, Cotesta S, Guagnano V, Rueeger H, Vaupel A. (2014). Preparation of Pyrazolopyrrolidine Derivatives as BET Inhibitors and Their Use in the Treatment of Cancers. U.S. Patent No US 2014/0349990 A1 Washington, DC: U.S. Patent and Trademark Office.
61. Schutzius G, Kolter C, Bergling S, Tortelli F, Fuchs F, Renner S, et al. BET Bromodomain Inhibitors Regulate Keratinocyte Plasticity. Nature Chem Biol (2021) 17(3):280–90. doi: 10.1038/s41589-020-00716-z. [PubMed: 33462494]
62. Richter A, Rose R, Hedberg C, Waldmann H, Ottmann C. An Optimised Small-Molecule Stabiliser of the 14-3-3-PMA2 Protein-Protein Interaction. Chem Eur J (2012) 18(21):6520–7, S/1–S/11. doi: 10.1002/chem.201103761. [PubMed: 22467351]
63. Mangiatordi GF, Trisciuzzi D, Alberga D, Denora N, Iacobazzi RM, Gadaleta D, et al. Novel Chemotypes Targeting Tubulin at the Colchicine Binding Site and Unbiasing P-Glycoprotein. Eur J Med Chem (2017) 139:792–803. doi: 10.1016/j.ejmech.2017.07.037. [PubMed: 28863359]
64. Zhou D, Bum-Erdene K, Xu D, Liu D, Tompkins D, Sulaiman RS, et al. Small Molecules Inhibit Ex Vivo Tumor Growth in Bone. Bioorg Med Chem (2018) 26(23–24):6128–34. doi: 10.1016/j.bmc.2018.11.025. [PubMed: 30470597]
65. Gunatilleke SS, Calvet CM, Johnston JB, Chen C-K, Erenburg G, Gut J, et al. Diverse Inhibitor Chemotypes Targeting *Trypanosoma cruzi* CYP51. PLoS Negl Trop Dis (2012) 6(7):e1736. doi: 10.1371/journal.pntd.0001736. [PubMed: 22860142]
66. Lamorte L, Titolo S, Lemke CT, Goudreau N, Mercier J-F, Wardrop E, et al. Discovery of Novel Small-Molecule HIV-1 Replication Inhibitors That Stabilize Capsid Complexes. Antimicrob Agents Chemother (2013) 57(10):4622–31. doi: 10.1128/AAC.00985-13. [PubMed: 23817385]
67. Lepage O, Bhardwaj PK, Faucher A-M, Grand-Maitre C, Lacoste J-E, Lamorte L. (2011). Pyrrolopyrazole Derivatives as HIV Replication Inhibitors and Use for the Treatment of HIV Infection. International Patent No WO 2011/143772 A1. Geneva, Switzerland: World Intellectual Property Organization.
68. Tang H, Lee EM, Zheng W, Huang R, Xu M, Huang W, et al. (2020). Anti-Flavivirus Compounds and Methods of Use. International Patent No WO 2020/132278 A1. Geneva, Switzerland: World Intellectual Property Organization.
69. Scharf NT, Molodtsov V, Kontos A, Murakami KS, Garcia GA. Novel Chemical Scaffolds for Inhibition of Rifamycin-Resistant Rna Polymerase Discovered from High-Throughput Screening. SLAS Discovery (2017) 22(3):287–97. doi: 10.1177/2472555216679994. [PubMed: 28027449]
70. Ballell L, Bates RH, Young RJ, Alvarez-Gomez D, Alvarez-Ruiz E, Barroso V, et al. Fueling Open-Source Drug Discovery: 177 Small-Molecule Leads against Tuberculosis. ChemMedChem (2013) 8(2):313–21. doi: 10.1002/cmdc.201200428. [PubMed: 23307663]
71. Barale J-C, Bouillon A, Giganti D, Gorgette OLG, Stoven V, Nilges M, et al. (2012). Screening Methods for Identifying Plasmodium Proteases Inhibitors. International Patent No WO 2012/073066 A1. Geneva, Switzerland: World Intellectual Property Organization.
72. Barale J-C, Bouillon A, Giganti D, Gorgette OLG, Stoven V, Nilges M, et al. (2011). Plasmodium Proteases Inhibitors and in Silico Screening Methods for Identifying the Same. Canada Patent No CA 2686584 A1. Quebec, Canada: Canadian Intellectual Property Office.
73. Anthouard R, DiRita VJ. Small-Molecule Inhibitors of toxT Expression in *Vibrio cholerae*. MBio (2013) 4(4):e00403. doi: 10.1128/mBio.00403-13. [PubMed: 23919997]
74. Kai H, Taoda Y, Endoh T, Horiguchi T, Asahi K, Tobinaga H (2010). Preparation of Novel Pyrrolinone and 4,5-Dihydro-1H-Pyrrolo[3,4-c]Pyrazol-6-One Derivatives as Purinoceptor Antagonists. International Patent No WO 2010/035727 A1. Geneva, Switzerland: World Intellectual Property Organization.
75. Kalid O, Mense M, Fischman S, Shitrit A, Bihler H, Ben-Zeev E, et al. Small Molecule Correctors of F508del-CFTR Discovered by Structure-Based Virtual Screening. J Comput-Aided Mol Des (2010) 24(12):971–91. doi: 10.1007/s10822-010-9390-0. [PubMed: 20976528]
76. Liu Z, Singh SB, Zheng Y, Lindblom P, Tice C, Dong C, et al. Discovery of Potent Inhibitors of 11β-Hydroxysteroid Dehydrogenase Type 1 Using a Novel Growth-Based Protocol of in Silico Screening and Optimization in Contour. J Chem Inf Model (2019) 59(8):3422–36. doi: 10.1021/acs.jcim.9b00198. [PubMed: 31355641]

Author Manuscript Author Manuscript Author Manuscript Author Manuscript

77. Pena I, Pilar Manzano M, Cantizani J, Kessler A, Alonso-Padilla J, Bardera AI, et al. New Compound Sets Identified from High Throughput Phenotypic Screening against Three Kinetoplastid Parasites: An Open Resource. Sci Rep (2015) 5:8771. doi: 10.1038/srep08771. [PubMed: 25740547]

Author Manuscript Author Manuscript Author Manuscript Author Manuscript

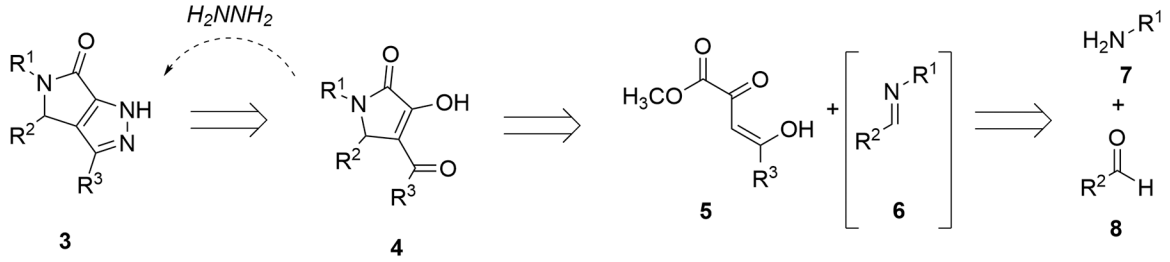

Figure 1.

Retrosynthetic route to produce pyrazolopyrrolidinones of structural type **3**

Author Manuscript Author Manuscript Author Manuscript Author Manuscript

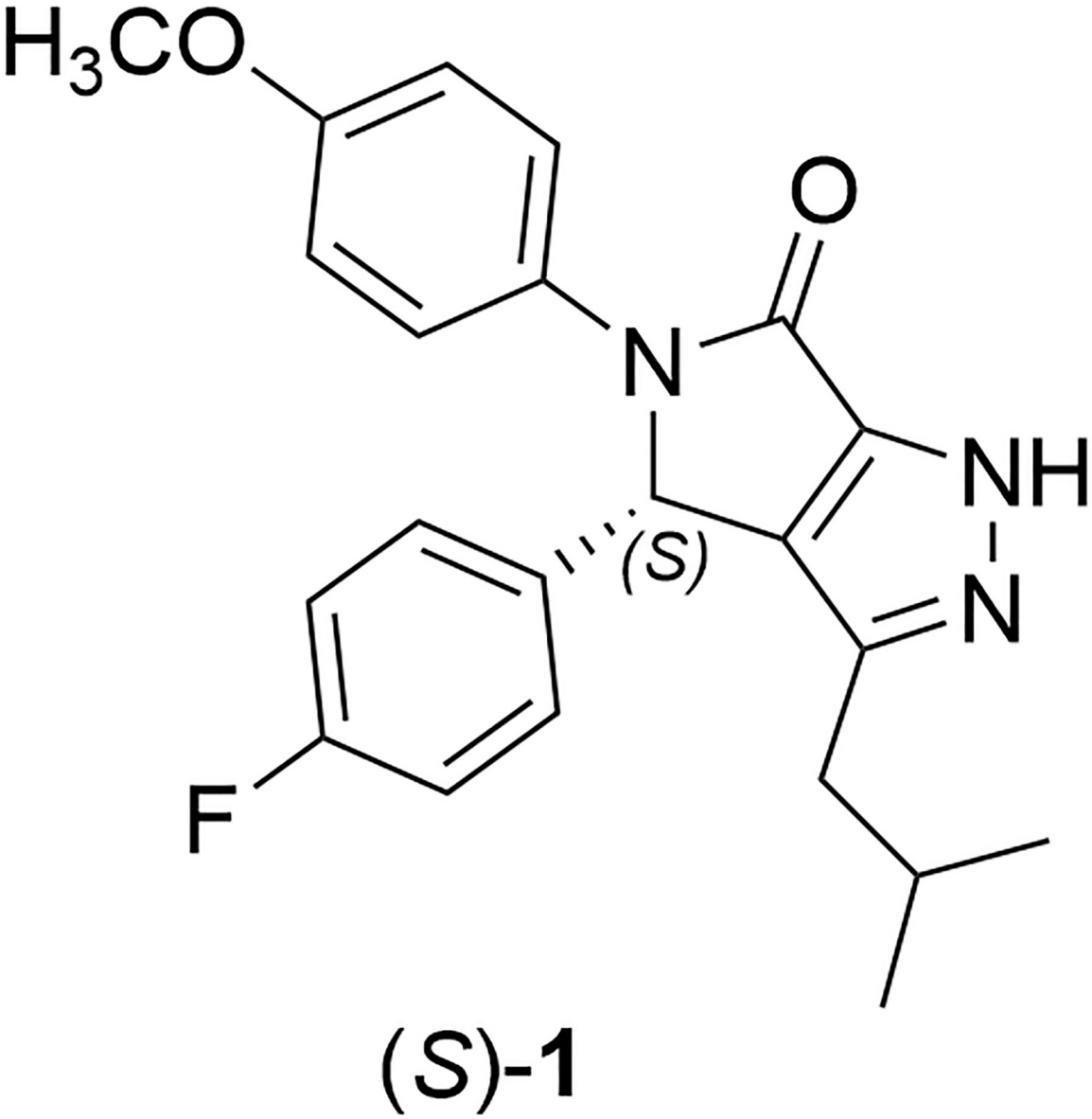

Figure 2.
Active (*S*) enantiomer of compound **1** as determined by VCD analysis

Author Manuscript

Author Manuscript

Author Manuscript

Author Manuscript

Table 1.

Structures and antiparasitic activity profiles of antileishmanial pyrazolopyrrolidinones **1** and **2**, first identified in a CDIPD (UCSF) high content screen for compounds inhibiting growth of *L. donovani* intracellular amastigotes infecting THP-1 cells.

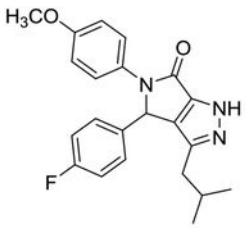

CMLD007431

1

CMLD007427

2

Compound	**Intracellular Amastigote EC_{50}**	**Extracellular promastigote EC_{50}**
Leishmania donovani		
CMLD007431 (**1**)	2.5 μM	2.0 μM
CMLD007427 (**2**)	3.7 μM	2.4 μM
Leishmania major		
CMLD007431 (**1**)	1.3 μM	4.4 μM
CMLD007427 (**2**)	1.7 μM	4.2 μM
Host (THP-1) cell CC_{50}		
CMLD007431 (**1**)	>20 μM	
CMLD007427 (**2**)	>20 μM	

Author Manuscript Author Manuscript Author Manuscript Author Manuscript

Table 2.

GlaxoSmithKline lead selection criteria for leishmaniasis

	Lead selection criteria	Compound 1	Criteria
***IN VITRO* EFFICACY**			
Antiparasitic activity	EC_{50} < 1 μM for *L. donovani* amastigotes	EC_{50} = 0.8 μM[a]; 2.5 μM[b]	Ideal
SI (HepG2, THP-1)[c]	> 50	HepG2 CC_{50} = 63.1 μM[a], SI(HepG2) = 79[a]; THP-1 CC_{50} = 31.6 μM[a,d]; SI(THP-1) = 40[a]	Accepted
DEVELOPABILITY			
MW	< 500 (< 420 ideally)	379	Ideal
PFI	≤ 7	8.4	Accepted
Aromatic rings	≤ 4 (ideally ≤3)	3	Ideal
Chemical Tractability	The chemical series is amenable to rapid analogues synthesis. Scale-up of potential lead (>1g with >95% purity) + consideration of cost of goods.	Pass	Ideal
***IN VITRO* ADME** [b]			
Solubility:			Ideal
CLND (μM)	> 30	107	
FaSSIF solubility (μg/mL)	> 5	130	
Microsomal stability (mouse)	Cl_{int} < 5 mL/min/g $t_{1/2}$ > 13.5 min	Cl_{int} < 3.4 mL/min/g $t_{1/2}$ > 20 min	Ideal
Whole blood stability	No % reduction over 120 min; No reactive functionalities	Pass	Ideal
Plasma protein binding	< 95%	97.5%	Accepted

[a.] Measured on the single enantiomer (*S*)-**1**.

[B.] Measured on the racemate (*rac*)-**1**.

[c.] SI = selectivity index compared to mammalian cells, calculated as SI = [mammalian cell CC_{50}] / [antiparasitic EC_{50}].

[d.] THP-1 cytotoxicity as measured in the GlaxoSmithKline LD AMMAC assay.

Author Manuscript Author Manuscript Author Manuscript Author Manuscript

Table 3:

Surveying the effects of variations at R^3. Values highlighted in **red** are considered improved in comparison to initial lead compound *rac*-**1**.

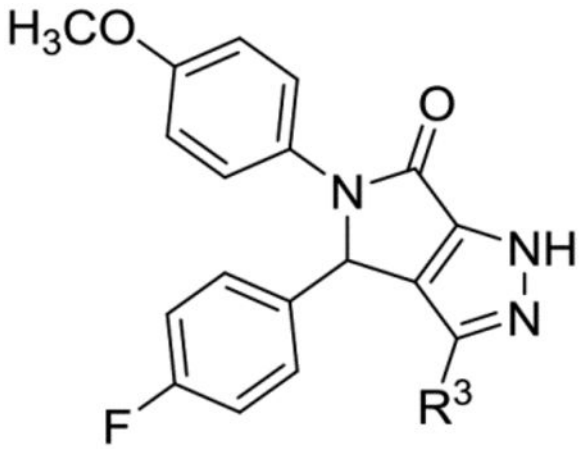

Cpd	R^3	LD AMMAC EC_{50} (μM)[a]	LD MAC EC_{50} (μM)[b]	SI MAC[c]	HEPG2 EC_{50} (μM)	Solubility[d] (μM)	AMP[e] (nm/sec)	HSA[f] Binding (%)	PFI[g]
***rac*-1**	isobutyl	2.5	15.8	6.3	63.1	107	345	96.4	8.4
9	isopentyl	2.5	31.6	12.6	79.4	15	100	98.0	9.1
10	neopentyl	2.5	25.1	10.0	39.8	36	170	97.4	9.0
11	*n*-butyl	0.1	2.5	25.0	50.1	49	370	96.7	8.4
12		1.6	3.2	2.0	50.1	135	410	97.5	8.1
13	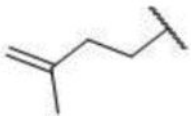	0.5	1.6	3.2	50.1	52	370	96.8	8.5
14	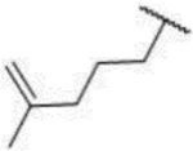	6.3	20.0	3.2	50.1	17	270	97.9	8.9
15	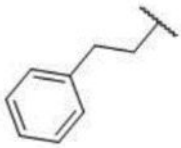	6.3	25.1	4.0	50.1	6	360	98.0	9.7

Author Manuscript Author Manuscript Author Manuscript Author Manuscript

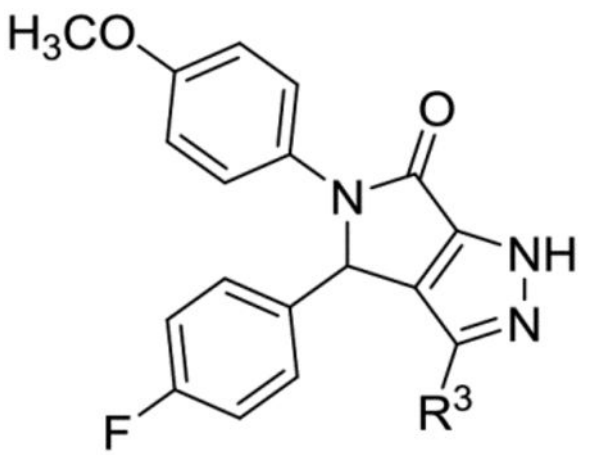

Cpd	R^3	LD AMMAC EC_{50} (μM)[a]	LD MAC EC_{50} (μM)[b]	SI MAC[c]	HEPG2 EC_{50} (μM)	Solubility[d] (μM)	AMP[e] (nm/sec)	HSA[f] Binding (%)	PFI[g]
16	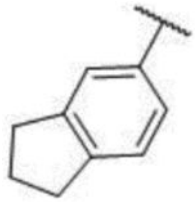	5.0	7.9	1.6	25.1	17	130	97.8	10.6
17	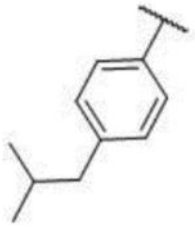	4.0	7.9	2.0	15.8	<1	340	98.0	11.4

[a] EC_{50} for growth inhibition of *L. donovani* intracellular amastigotes infecting THP-1 macrophages;

[b] EC_{50} for cytotoxicity against host THP-1 macrophages;

[c] SI MAC = selectivity index in macrophages, calculated as SI MAC = (LD MAC EC_{50})/(LD AMMAC EC_{50});

[d] kinetic aqueous solubility as determined by high-throughput CLND (chemoluminescent nitrogen detection);

[e] artificial membrane permeability;

[f] human serum albumin binding;

[g] PFI = $ChromLogD_{7.4}$ + Aromatic rings

Author Manuscript Author Manuscript Author Manuscript Author Manuscript

Table 4:

Surveying effects of various *p*-substituted aromatics at R^1. Values highlighted in **red** are considered improved in comparison to initial lead compound **1**.

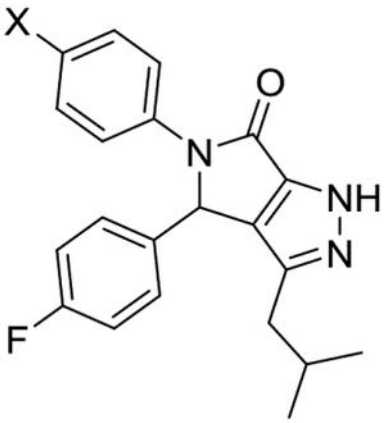

Compound	X	LD AMMAC EC_{50} (μM)[a]	LD MAC EC_{50} (μM)[b]	SI MAC[c]	HEPG2 EC_{50} (μM)	Solubility[d] (μM)	AMP[e] (nm/sec)	HSA[f] Binding (%)	PFI[g]
1	$-OCH_3$	2.5	15.8	6.3	63.1	107	345	96.4	8.4
18	-OH	5.0	39.8	8.0	>100	≥430	285	95.6	7.1
19	-OEt	1.6	20.0	12.5	50.1	38	250	97.5	8.9
20	$-OCF_3$	3.2	7.9	2.5	25.1	5	290	98.1	9.8
21	$-N(CH_3)_2$	1.0	39.8	39.8	50.1	33	160	96.1	9.0
22	-Et	4.0	20.0	5.0	50.1	9	<10	97.4	9.7
23	-F	6.3	25.1	4.0	50.1	61	120	97.7	8.8
24	-Br	1.3	15.8	12.2	39.8	9	320	97.9	9.7
25	-*t*-Bu	10.0	>50	>5.0	50.1	<1	130	97.9	10.5
26	$-CO_2CH_3$	1.6	31.6	20.0	39.8	26	410	97.5	8.5
27	$-CO_2H$	>50	>50	n/a	>100	≥389	<3	95.2	4.9
28	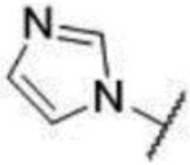	2.5	>50	>20.0	>100	7	<3	96.3	8.1

[a] EC_{50} for growth inhibition of *L. donovani* intracellular amastigotes infecting THP-1 macrophages;

[b] EC_{50} for cytotoxicity against host THP-1 macrophages;

[c] SI MAC = selectivity index in macrophages, calculated as SI MAC = (LD MAC EC_{50})/(LD AMMAC EC_{50});

[d] kinetic aqueous solubility as determined by high-throughput CLND (chemoluminescent nitrogen detection);

[e] artificial membrane permeability;

[f] human serum albumin binding;

[g] PFI = ChromLogD$_{7.4}$ + Aromatic rings

Author Manuscript Author Manuscript Author Manuscript Author Manuscript

Author Manuscript Author Manuscript Author Manuscript Author Manuscript

Table 5:

Probing expanded diversity at R^1. Values highlighted in **red** are considered improved in comparison to initial lead compound **1**.

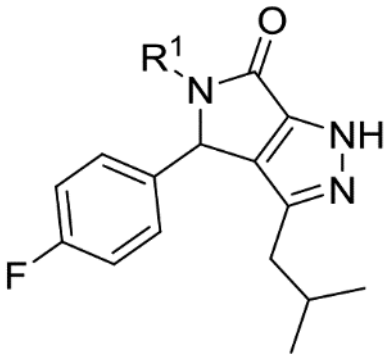

Cpd	R^1	LD AMMAC EC_{50} (μM)[a]	LD MAC EC_{50} (μM)[b]	SI MAC[c]	HEPG2 EC_{50} (μM)	Solubility[d] (μM)	AMP[e] (nm/sec)	HSA[f] Binding (%)	PFI[g]
1	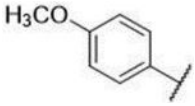	2.5	15.8	6.3	63.1	107	345	96.4	8.4
29	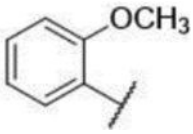	20.0	>50	>2.5	79.4	240	590	97.5	8.5
30	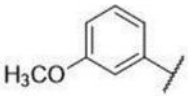	12.6	31.6	2.5	63.1	64	370	97.3	8.4
31	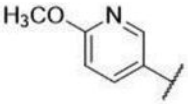	10.0	>50	>5.0	>100	194	260	95.5	8.0
32	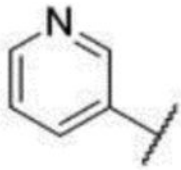	25.1	>50	>2.0	>100	182	470	93.4	7.2

Author Manuscript Author Manuscript Author Manuscript Author Manuscript

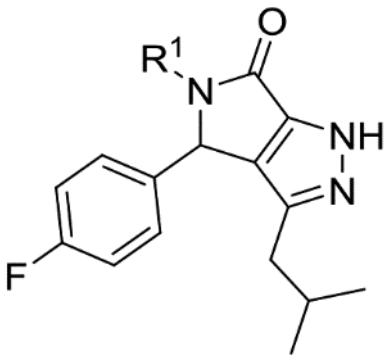

Cpd	R^1	LD AMMAC EC_{50} (μM)[a]	LD MAC EC_{50} (μM)[b]	SI MAC[c]	HEPG2 EC_{50} (μM)	Solubility[d] (μM)	AMP[e] (nm/sec)	HSA[f] Binding (%)	PFI[g]
33	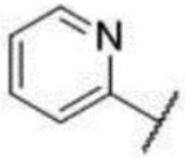	20.0	>50	>2.5	>100	219	200	96.6	8.5
34	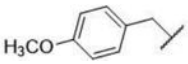	12.6	31.6	>2.5	50.1	45	550	98.2	9.0
35	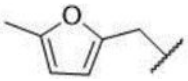	15.8	39.8	>2.5	50.1	19	370	97.2	8.9
36	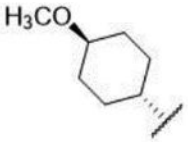	25.1	>50	>2.0	>100	≥450	570	92.1	7.3
37	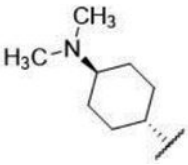	25.1	>50	>2.0	>100	≥446	130	81.1	4.6
38	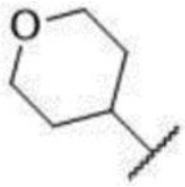	31.6	>50	>1.6	>100	≥381	490	90.2	6.5

Author Manuscript Author Manuscript Author Manuscript Author Manuscript

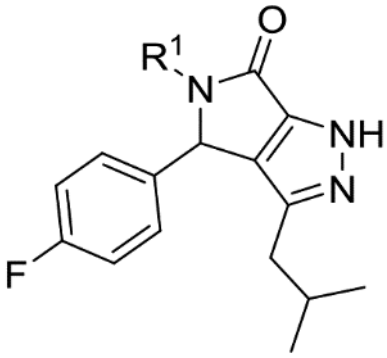

Cpd	R[1]	LD AMMAC EC_{50} (μM)[a]	LD MAC EC_{50} (μM)[b]	SI MAC[c]	HEPG2 EC_{50} (μM)	Solubility[d] (μM)	AMP[e] (nm/sec)	HSA[f] Binding (%)	PFI[g]
39	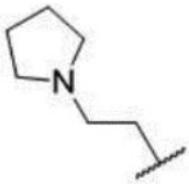	15.8	>50	>3.2	>100	≥433	230	76.7	5.3
40	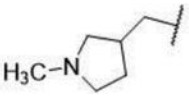	>50	>50	>1.0	>100	≥351	<10	77.5	4.8
41	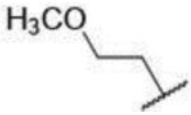	>50	>50	>1.0	>100	≥421	520	90.2	6.7

[(a)] EC_{50} for growth inhibition of *L. donovani* intracellular amastigotes infecting THP-1 macrophages;

[(b)] EC_{50} for cytotoxicity against host THP-1 macrophages;

[(c)] SI MAC = selectivity index in macrophages, calculated as SI MAC = (LD MAC EC_{50})/(LD AMMAC EC_{50});

[(d)] kinetic aqueous solubility as determined by high-throughput CLND (chemoluminescent nitrogen detection);

[(e)] artificial membrane permeability;

[(f)] human serum albumin binding;

[(g)] PFI = $ChromLogD_{7.4}$ + Aromatic rings.

Author Manuscript Author Manuscript Author Manuscript Author Manuscript

Table 6:

Surveying effects of di- and tri- substitutions at R^1. Values highlighted in **red** are considered improved in comparison to initial lead compound **1**.

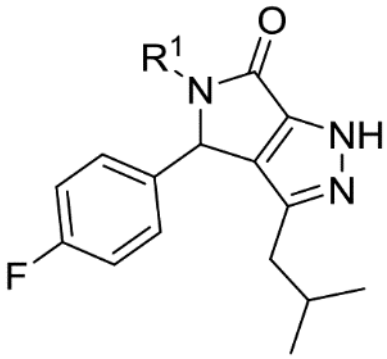

Cpd	R^1	LD AMMAC EC_{50} (μM)[a]	LD MAC EC_{50} (μM)[b]	SI MAC[c]	HEPG2 EC_{50} (μM)	Solubility[d] (μM)	AMP[e] (nm/sec)	HSA[f] Binding (%)	PFI[g]
1	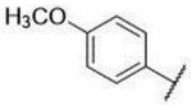	2.5	15.8	6.3	63.1	107	345	96.4	8.4
42	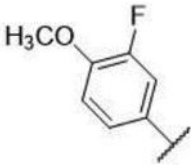	1.3	25.1	19.3	50.1	39	290	96.9	8.6
43	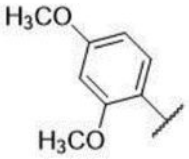	20.0	31.6	1.6	63.1	138	170	96.2	8.5
44	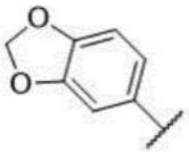	0.6	25.1	41.8	63.1	63	390	96.2	8.4
45	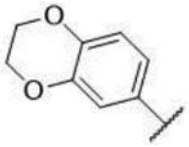	3.2	25.1	7.9	>50	50	510	96.2	8.4

Author Manuscript

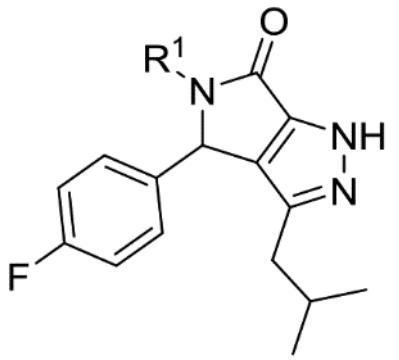

Cpd	R[1]	LD AMMAC EC_{50} (μM)[a]	LD MAC EC_{50} (μM)[b]	SI MAC[c]	HEPG2 EC_{50} (μM)	Solubility[d] (μM)	AMP[e] (nm/sec)	HSA[f] Binding (%)	PFI[g]
46	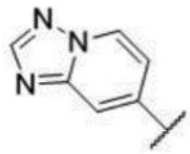	5.0	>50	>10	>50	49	920	91.8	7.8

[(a)] EC_{50} for growth inhibition of *L. donovani* intracellular amastigotes infecting THP-1 macrophages;

[(b)] EC_{50} for cytotoxicity against host THP-1 macrophages;

[(c)] SI MAC = selectivity index in macrophages, calculated as SI MAC = (LD MAC EC_{50})/(LD AMMAC EC_{50});

[(d)] kinetic aqueous solubility as determined by high-throughput CLND (chemoluminescent nitrogen detection);

[(e)] artificial membrane permeability;

[(f)] human serum albumin binding;

[(g)] PFI = $ChromLogD_{7.4}$ + Aromatic rings

Author Manuscript Author Manuscript Author Manuscript Author Manuscript

Table 7:

Surveying effects of simple aliphatic and aromatic R^2. Values highlighted in **red** are considered improved in comparison to initial lead compound **1**.

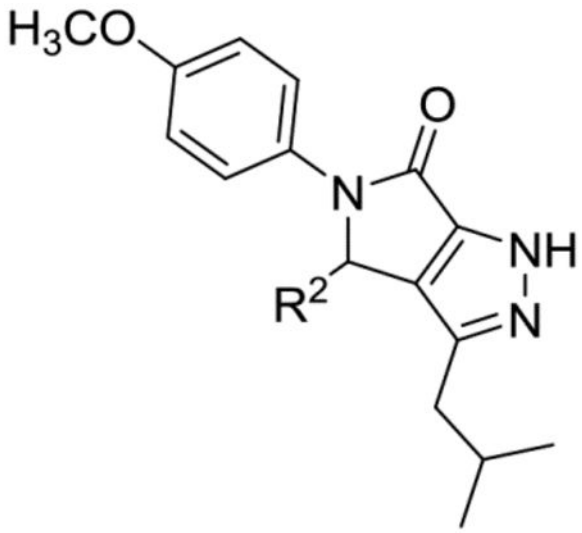

Cpd	R^2	LD AMMAC EC_{50} (μM)[a]	LD MAC EC_{50} (μM)[b]	SI MAC[c]	HEPG2 EC_{50} (μM)	Solubility[d] (μM)	AMP[e] (nm/sec)	HSA[f] Binding (%)	PFI[g]
1	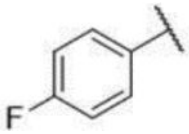	2.5	15.8	6.3	63.1	107	345	96.4	8.4
2	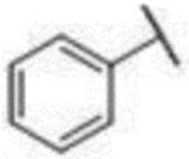	3.2	31.6	9.9	79.4	90	370	95.8	8.4
47	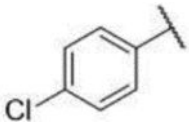	4.0	15.8	4.0	50.1	22	330	96.9	9.2
48	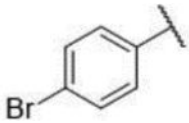	6.3	15.8	2.5	50.1	9	420	97.2	9.3

Author Manuscript Author Manuscript Author Manuscript Author Manuscript

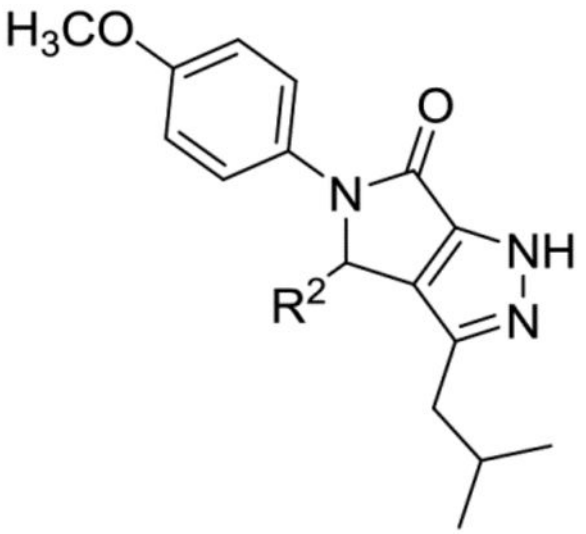

Cpd	R^2	LD AMMAC EC_{50} (μM)[a]	LD MAC EC_{50} (μM)[b]	SI MAC[c]	HEPG2 EC_{50} (μM)	Solubility[d] (μM)	AMP[e] (nm/sec)	HSA[f] Binding (%)	PFI[g]
49	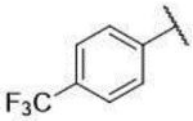	8.0	15.8	2.0	50.1	12	210	96.9	9.3
50	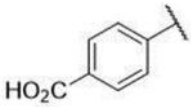	>50	>50	1.0	>100	≥470	<3	90.7	4.5
51	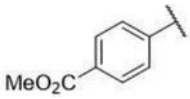	25.1	39.8	1.6	63.1	44	380	95	8.2
52	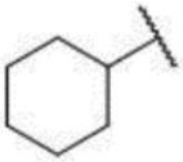	7.9	25.1	3.2	50.1	29	330	97.6	8.5
53	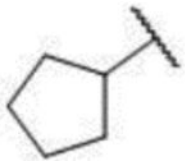	12.6	20.0	1.6	>100	119	590	96.3	8.1

Author Manuscript Author Manuscript Author Manuscript Author Manuscript

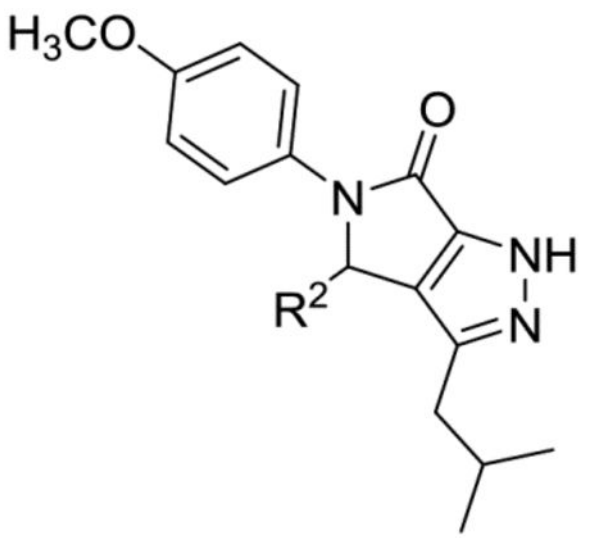

Cpd	R^2	LD AMMAC EC_{50} (μM)[a]	LD MAC EC_{50} (μM)[b]	SI MAC[c]	HEPG2 EC_{50} (μM)	Solubility[d] (μM)	AMP[e] (nm/sec)	HSA[f] Binding (%)	PFI[g]
54	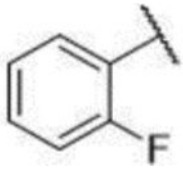	3.2	31.6	9.9	31.6	75	230	97.3	8.6
55	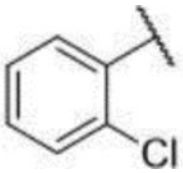	1.3	20.0	15.3	31.6	30	330	97.8	8.8
56	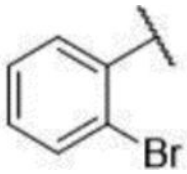	0.5	25.1	50.2	39.8	12	300	97.1	9.2
57	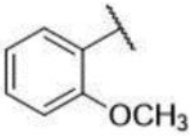	0.5	25.1	50.2	6.3	57	350	95.7	8.6

Author Manuscript Author Manuscript Author Manuscript Author Manuscript

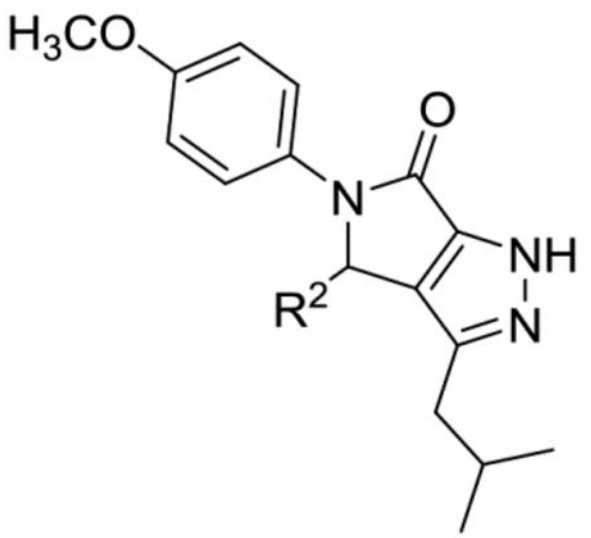

Cpd	R^2	LD AMMAC EC_{50} (μM)[a]	LD MAC EC_{50} (μM)[b]	SI MAC[c]	HEPG2 EC_{50} (μM)	Solubility[d] (μM)	AMP[e] (nm/sec)	HSA[f] Binding (%)	PFI[g]
58	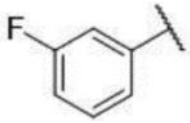	5.0	12.6	2.5	50.1	91	370	96.9	8.3
59	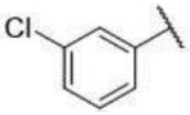	7.9	39.8	5.0	39.8	19	280	96.8	9.0
60	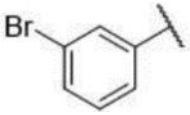	7.9	25.1	3.2	39.8	10	370	97	9.1
61	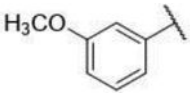	4.0	20.0	5.0	63.1	63	290	95	8.4
62	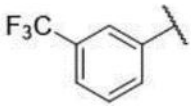	6.3	15.8	2.5	50.1	20	220	97.8	8.9
63	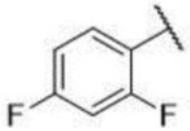	2.0	25.1	12.6	63.1	52	140	96.1	8.8

Author Manuscript Author Manuscript Author Manuscript Author Manuscript

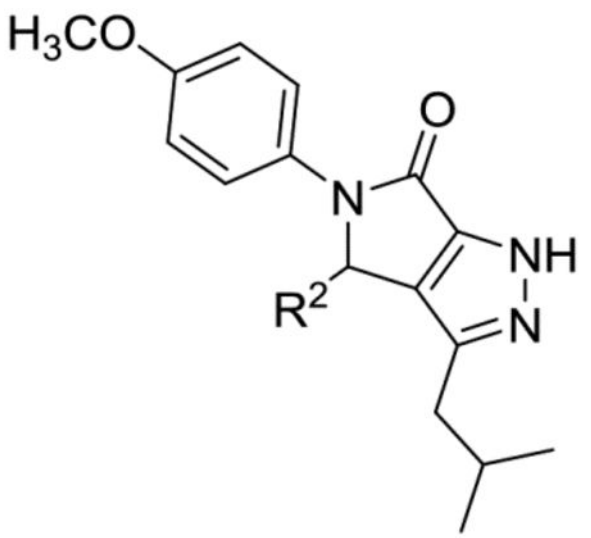

Cpd	R^2	LD AMMAC EC_{50} (μM)[a]	LD MAC EC_{50} (μM)[b]	SI MAC[c]	HEPG2 EC_{50} (μM)	Solubility[d] (μM)	AMP[e] (nm/sec)	HSA[f] Binding (%)	PFI[g]
64	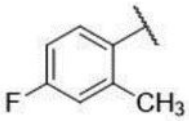	0.5	25.1	50.2	50.1	43	110	97.2	8.8
65	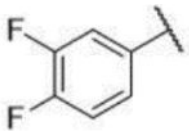	5.0	25.1	5.0	50.1	44	140	96.2	8.7
66	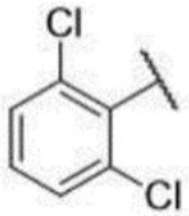	1.0	2.5	2.5	6.3	6	330	97.1	9.1

[a] EC_{50} for growth inhibition of *L. donovani* intracellular amastigotes infecting THP-1 macrophages;

[b] EC_{50} for cytotoxicity against host THP-1 macrophages;

[c] SI MAC = selectivity index in macrophages, calculated as SI MAC = (LD MAC EC_{50})/(LD AMMAC EC_{50});

[d] kinetic aqueous solubility as determined by high-throughput CLND (chemoluminescent nitrogen detection);

[e] artificial membrane permeability;

[f] human serum albumin binding;

[g] PFI = ChromLogD$_{7.4}$ + Aromatic rings

Author Manuscript Author Manuscript Author Manuscript Author Manuscript

Author Manuscript Author Manuscript Author Manuscript Author Manuscript

Table 8:

Pairing of promising R^1/R^2 moieties toward improved inhibitors. Values highlighted in red are considered improved in comparison to initial lead compound 1.

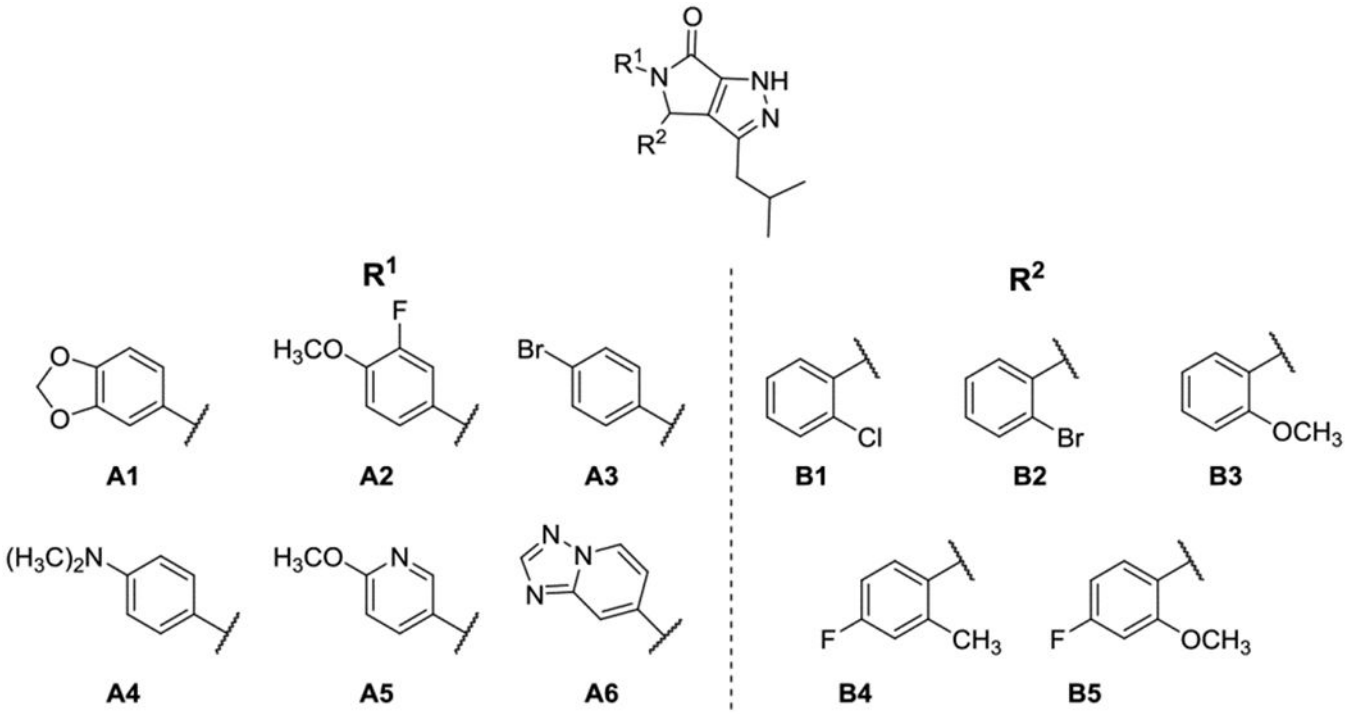

Cpd	R^1	R^2	*L. donovani* EC_{50} (μM)[a]	CC_{50} (μM)[b]	SI[c]	Solubility[d] (μM)	HSA[e] binding (%)	PFI[g]
(*rac*)-**1**	-	-	0.82	>20.00	>24.4	89[f]	96.4	8.4
67	**A1**	**B1**	0.16	12.22	76.4	35	98.0	8.7
68	**A1**	**B2**	0.29	>20.00	>69.0	27	97.0	8.8
69	**A1**	**B3**	0.27	>20.00	>74.1	66	95.3	8.2
70	**A1**	**B4**	0.10	12.08	120.8	46	97.6	8.6
71	**A2**	**B2**	0.42	3.04	7.2	20	96.9	9.2
72	**A2**	**B3**	0.38	0.26	0.7	43	95.9	8.5
73	**A2**	**B4**	0.16	10.89	68.1	35	96.3	8.8
74	**A3**	**B2**	0.39	4.98	12.8	<1	98.0	10.4
75	**A3**	**B3**	0.24	1.14	4.8	<1	97.5	9.6
76	**A3**	**B4**	0.12	3.04	25.3	<1	97.7	9.8
77	**A3**	**B5**	0.12	4.04	33.7	<1	98.5	9.7
78	**A4**	**B1**	0.26	7.32	28.2	21	96.7	9.4
79	**A4**	**B2**	0.08	5.72	71.5	<1	96.9	9.4
80	**A4**	**B3**	0.07	3.45	49.3	66	95.7	8.6
81	**A4**	**B4**	0.11	7.51	68.3	27	96.5	9.1

Author Manuscript Author Manuscript Author Manuscript Author Manuscript

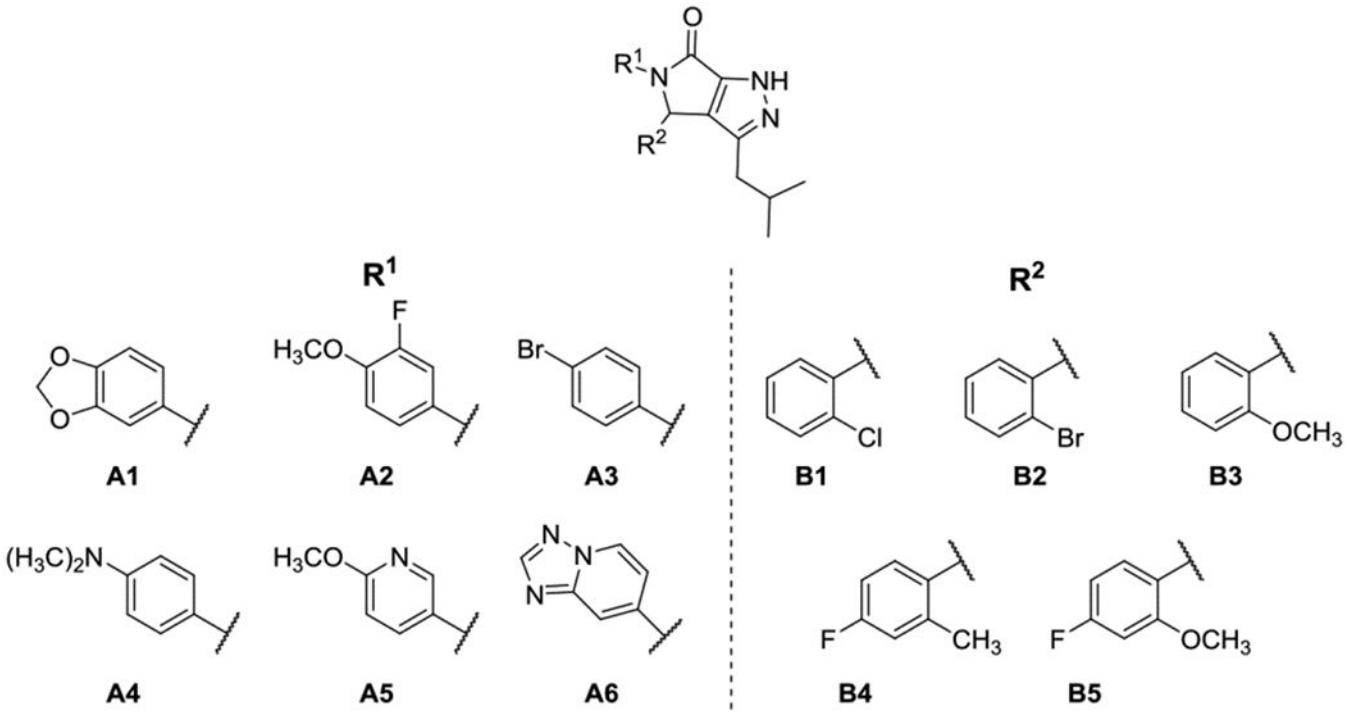

Cpd	R^1	R^2	*L. donovani* EC_{50} (μM)[a]	CC_{50} (μM)[b]	SI[c]	Solubility[d] (μM)	HSA[e] binding (%)	PFI[g]
82	**A4**	**B5**	0.04	8.50	212.5	45	97.1	8.8
83	**A5**	**B1**	1.11	9.93	8.9	77	97.0	8.7
84	**A5**	**B2**	0.98	>20.00	>54.1	63	96.6	8.8
85	**A5**	**B3**	1.11	>20.00	>76.9	176	93.9	8.0
86	**A5**	**B4**	0.37	>20.00	>36.4	119	94.7	8.3
87	**A5**	**B5**	0.26	>20.00	>23.0	145	94.1	8.1
88	**A6**	**B1**	0.55	>20.00	>55.6	<1	94.1	8.0
89	**A6**	**B4**	0.87	>20.00	>24.4	<1	93.2	8.1

[(a)] EC_{50} for growth inhibition of *L. donovani* intracellular amastigotes infecting B10R cells (UCSD assay), average of two biological replicates;

[(b)] EC_{50} for cytotoxicity against host B10R cells (UCSD assay);

[(c)] SI = selectivity index, calculated as SI = (*L. donovani* infection EC_{50})/(CC_{50});

[(d)] kinetic aqueous solubility as determined by high-throughput CAD (charged aerosol detection);

[(e)] human serum albumin binding.

[(f)] Obtained on the single enantiomer (*S*)-**1**;

[(g)] PFI = $ChromLogD_{7.4}$ + Aromatic rings